

New Physics in $B_q^0-\bar{B}_q^0$ Mixing: Present Challenges, Prospects, and Implications for $B_q^0 \rightarrow \mu^+\mu^-$

Kristof De Bruyn ^{a,b}, Robert Fleischer ^{a,c}, Eleftheria Malami ^a
and Philine van Vliet ^d

^a*Nikhef, Science Park 105, 1098 XG Amsterdam, Netherlands*

^b*Van Swinderen Institute for Particle Physics and Gravity, University of Groningen,
9747 Groningen, Netherlands*

^c*Faculty of Science, Vrije Universiteit Amsterdam,
1081 HV Amsterdam, Netherlands*

^d*Deutsches Elektronen-Synchrotron DESY, Notkestr. 85, 22607 Hamburg, Germany*

Abstract

The phenomenon of $B_q^0-\bar{B}_q^0$ mixing ($q = d, s$) provides a sensitive probe for physics beyond the Standard Model. We explore the corresponding space for New Physics left through the current data, having a careful look at analyses of the Unitarity Triangle that are needed for the Standard Model predictions of the B_q mixing parameters. In particular, we explore the impact of tensions between inclusive and exclusive determinations of the CKM matrix elements $|V_{ub}|$ and $|V_{cb}|$. Moreover, we focus on the angle γ of the Unitarity Triangle, comparing measurements from $B \rightarrow DK$ and $B \rightarrow \pi\pi, \rho\pi, \rho\rho$ decays, where the latter are typically interpreted in terms of the angle α . We discuss various scenarios and present the corresponding state-of-the-art constraints on the New Physics parameters of $B_q^0-\bar{B}_q^0$ mixing. We point out that these results have an interesting application in the analysis of rare $B_q^0 \rightarrow \mu^+\mu^-$ decays, allowing us to minimise the impact of CKM parameters in the search for New Physics. In view of the high-precision era, we make future projections. Interestingly, we find that for the extraction of the New Physics parameters in the B_d system the determination of the apex of the Unitarity Triangle results in a key limiting factor. By contrast, the corresponding impact is negligible for the B_s system, making it a promising candidate to reveal sources of New Physics.

1 Introduction

Mixing between neutral B_q^0 and \bar{B}_q^0 mesons, where q can be either a down or a strange quark, offers interesting opportunities to test the Standard Model (SM) paradigm at energy scales well beyond the centre-of-mass energy of the Large Hadron Collider (LHC). The mixing process is an example of a flavour-changing neutral current and proceeds via box diagrams, which are loop-suppressed. This makes it an ideal place to search for the effects of New Physics (NP) contributions. The parameter space for NP in B_q -meson mixing can be determined in a model-independent way [1], and has been analysed in the past [2–7]. But, as we will demonstrate below, the values of the SM predictions for the mixing phases and amplitudes strongly depend on our choices for the input measurements, and in particular on the determination of the apex of the Unitarity Triangle (UT). The searches for NP in B_q -meson mixing thus critically rely on resolving various tensions between measurements of the elements of the Cabibbo–Kobayashi–Maskawa (CKM) quark mixing matrix [8, 9]. In this paper, we will demonstrate the impact that the different experimental measurements related to the CKM matrix and UT have on the parameter space for NP in B_q^0 – \bar{B}_q^0 mixing. In addition, we will compare the results for NP in B_d^0 – \bar{B}_d^0 and B_s^0 – \bar{B}_s^0 mixing with each other, highlighting the similarities as well as differences between the two systems.

The allowed parameter space for NP in B_q -meson mixing is impacted by two important subtleties regarding the determination of the UT apex, which are both currently at risk of being overlooked. The first subtlety is due to existing discrepancies between the measurements of individual input parameters, while the second subtlety is related to our choice of inputs to determine the apex of the UT. Key examples regarding the first point are the measurements of the CKM matrix elements $|V_{cb}|$ and $|V_{ub}|$. Despite the best efforts from experts in the field, we have not yet been able to resolve the discrepancies between the inclusive and exclusive determinations of these quantities (see Ref. [10] for a review). The numerical differences between both determinations directly affect many SM predictions in flavour physics, including those related to B_q^0 – \bar{B}_q^0 mixing. These differences should therefore not be ignored, as would be the case when naively averaging the results from both measurement strategies. Instead, at each step of our analysis, we will demonstrate what impact the difference between the inclusive and exclusive determinations of $|V_{cb}|$ and $|V_{ub}|$ has on the results.

Secondly, to constrain the parameter space for NP in B_q^0 – \bar{B}_q^0 mixing, it is of utmost importance to understand how the different input measurements can be affected by NP contributions themselves. Global analyses that assume SM expressions, like those performed by the CKMfitter [11] or UTfit [12] groups, combine information from all relevant input measurements to determine the UT apex. However, each of the individual experimental inputs can, in principle, be affected by different NP contributions, clouding the resulting picture of the UT apex. As such, the obtained fit solution cannot reliably be used to make SM predictions. Global fits allowing for NP effects in the inputs have been made [3, 6]. However, in this work we will only focus on NP in B_q^0 – \bar{B}_q^0 mixing.

Not all experimental inputs are equally sensitive or equally affected by NP contributions. Observables which can be measured through decays dominated by tree-level topologies, such as the UT side R_b and the UT angle γ , are typically considered less prone to NP effects, while observables affected by loop-level processes, such as the UT angle β and the mass difference Δm_s between the mass eigenstates of the B_s -meson sys-

tem, are considered to be much more sensitive. For SM calculations, the use of the latter category should therefore be avoided. Since our main goal is to study NP in B_q -meson mixing, we especially have to make sure to use input measurements free of possible contributions from NP in $B_q^0\text{--}\bar{B}_q^0$ mixing. For that reason, we will perform and discuss our own fits of the UT apex, which aim to be completely transparent with respect to which input measurements are used and how they could be affected by NP.

Our SM determination of the UT apex uses only two observables: the UT side R_b and the UT angle γ , to keep possible contamination of the input parameters due to NP to a minimum. Both these observables are affected by the subtleties introduced above and thus require a careful analysis. The numerical value for R_b strongly depends on our choice for the CKM matrix elements $|V_{cb}|$ and $|V_{ub}|$, propagating the unresolved discrepancies between the inclusive and exclusive determinations to the solution for the UT apex, and to the SM predictions of the B_q -meson mixing parameters. For γ , on the other hand, there are multiple strategies from a variety of B -meson decay channels to measure its value. The most precise direct determination of γ is obtained from a combination of multiple CP violation measurements in the $B \rightarrow DK$ family of decays [13]. These channels proceed via tree topologies only. In most beyond the SM theories, the NP contributions are strongly suppressed in these topologies, and can thus still be neglected. Nonetheless, it remains possible for NP effects to be present in these decays [14–18]. Therefore it is important to carefully compare the results from individual measurements, now and in the future, and in particular when including them in experimental averages. In this respect, the decay-time-independent measurements using B^+ and B_d^0 decays show an interesting difference compared to the decay-time-dependent measurement in the $B_s^0 \rightarrow D_s^\mp K^\pm$ channel [19,20].

In addition, a second high-precision measurement of γ can be obtained from the isospin analysis of the $B \rightarrow \pi\pi$, $\rho\pi$, $\rho\rho$ decays. This analysis is commonly presented as a measurement of the UT angle α , but we argue that, in view of NP searches, it is natural and more advantageous to interpret it as a measurement of γ . In contrast to the $B \rightarrow DK$ decays, the $B \rightarrow \pi\pi$, $\rho\pi$, $\rho\rho$ modes also get contributions from loop-level penguin topologies. The isospin relations between the three decay modes allow us to control the size of these penguin topologies, and take into account their impact on the determination of the UT angle γ . In the literature, this relation is usually used to obtain a measurement of α , assuming $\alpha + \beta + \gamma = 180^\circ$. However, in this paper, we will not make this assumption and instead consider the isospin relations as an independent determination of γ , using experimental input from the $B_d^0\text{--}\bar{B}_d^0$ mixing phase ϕ_d , which is given by 2β in the SM. It should be stressed that the underlying physics processes are vastly different from the $B \rightarrow DK$ decays, and a comparison of the results is therefore highly non-trivial. If the two obtained values for γ agree with each other, this would place the determination of the UT apex via R_b and γ on a more robust footing, while in case they disagree, one would have a clear indicator for possible NP. This also illustrates that we need to be very careful when making averages of different measurements, and this should only be done after proper justification.

After a careful analysis of the UT apex focused on providing clean SM predictions for the B_q -meson mixing parameters, we discuss the parameter space that is still left for NP. Here, we will consider three different scenarios. The first uses R_b and γ as input for the SM predictions and determines the parameter space for NP separately for the B_d and B_s systems. This is the most general scenario and serves as a baseline for a comparison with the other two options. The only assumptions are that R_b and γ are

free of possible NP. The purpose of the other two scenarios is to investigate what impact additional assumptions can have on the allowed parameter space for NP in B_q mixing. We will name the second scenario that we consider Flavour Universal New Physics (FUNP), where the NP in the B_d and the B_s system is assumed to be equal. In this case, also the ratio between the mixing parameters Δm_d and Δm_s is free from NP, and can be used to determine the side R_t of the UT. Combining it with the side R_b , it is then possible to obtain the SM UT apex without relying on γ . By comparing this scenario to the baseline, we can see how compatible the data are with the FUNP assumption. The third scenario is a mixture of the previous two, where we assume FUNP in the determination of the UT apex, but do not impose this condition when determining the space left for NP in B_d and B_s mixing separately. Comparing these results with those from the other two scenarios gives us insights into the impact that the UT apex has on the NP searches in $B_q^0\text{--}\bar{B}_q^0$ mixing.

The unresolved discrepancies between the measurements of the CKM matrix elements not only impact the determination of the UT apex and the NP searches in $B_q^0\text{--}\bar{B}_q^0$ mixing, but also affect other high-profile NP searches. One particularly interesting example is the branching fraction measurement of the rare decay $B_s^0 \rightarrow \mu^+\mu^-$, which originates from $b \rightarrow s\ell\ell$ flavour changing neutral current processes. We will illustrate how our choices for $|V_{ub}|$ and $|V_{cb}|$ propagate to the allowed parameter space for the pseudo-scalar and scalar NP contributions in $B_s^0 \rightarrow \mu^+\mu^-$. The dependence on these CKM matrix elements can be minimised, as was pointed out in Refs. [21–23], by taking the ratio between the $B_s^0 \rightarrow \mu^+\mu^-$ branching fraction and the mixing parameter Δm_s . Using this ratio to search for NP in the decay of $B_s^0 \rightarrow \mu^+\mu^-$ does require to take into account the NP contributions in $B_q^0\text{--}\bar{B}_q^0$ mixing. We therefore apply our results from the general, model-independent NP fit to illustrate how this ratio offers an interesting alternative constraint on the pseudo-scalar and scalar NP contributions. All these considerations can also be applied to the $B_d^0 \rightarrow \mu^+\mu^-$ decay once accurate branching fraction measurements become available in the future.

The outline of this paper is as follows: We start our analysis in Section 2 with a discussion on the input measurements of γ and R_b , fit the UT apex, and compare our solution with the constraint following from $|\varepsilon_K|$, describing indirect CP violation in the neutral kaon system, which is highly sensitive to $|V_{cb}|$. Next, in Section 3 we introduce the SM $B_q^0\text{--}\bar{B}_q^0$ mixing observables, which we need as reference to constrain the parameter space for NP. In addition, we use the ratio between the mixing parameters Δm_s and Δm_d to obtain an alternative solution for the UT apex that can be used for SM predictions under the assumption of FUNP. This alternative solution will be used in our NP search. The three scenarios for NP in $B_q^0\text{--}\bar{B}_q^0$ mixing are discussed in Section 4, and the applications for the rare decay $B_q^0 \rightarrow \mu^+\mu^-$ in Section 5. In Section 6, we explore and illustrate the impact of increased precision on the key input measurements in the future. Finally, we conclude in Section 7.

2 Determination of the UT Apex

The NP searches in $B_q^0\text{--}\bar{B}_q^0$ mixing require accurate SM predictions of the mixing parameters (see Section 3). Their SM values depend on the apex $(\bar{\rho}, \bar{\eta})$ of the UT, where

$$\bar{\rho} \equiv \left(1 - \frac{\lambda^2}{2}\right) \rho, \quad \bar{\eta} \equiv \left(1 - \frac{\lambda^2}{2}\right) \eta, \quad (1)$$

and λ , ρ and η are three of the Wolfenstein parameters [24,25]. The UT apex thus plays a crucial role in the analysis, but we cannot rely on global fits of the UT [11,12] to calculate the SM values, as they include input measurements that are potentially affected by NP in $B_q^0\text{--}\bar{B}_q^0$ mixing, and would thus bias our results. Instead, we will only use information on the side R_b and the angle γ to determine $\bar{\rho}$ and $\bar{\eta}$. Using the Particle Data Group [26] parametrisation of the CKM matrix, the coordinates of the UT apex are given by

$$R_b e^{i\gamma} = \bar{\rho} + i\bar{\eta}, \quad (2)$$

where R_b and γ will be defined in more detail below. The advantage of this approach is that R_b and γ can be determined from decays that proceed via tree topologies only. In general, NP contributions are considered to be strongly suppressed in tree topologies, which are thus less sensitive to their effects. Measurements of the ratios of semileptonic branching fractions $R(D)$ and $R(D^*)$ [27] might contest this assumption [28–31]. Interestingly, NP effects can be included in these decays and the corresponding determination of the CKM matrix elements [32–35]. If NP enters only through couplings to heavy τ leptons, the determinations of $|V_{cb}|$ and $|V_{ub}|$ from semileptonic B decays into the light leptons $\ell = e, \mu$, which are the only determinations of these CKM matrix elements used in this paper, would be as in the SM. Since the determination of γ uses non-leptonic decays, and the determination of R_b does not rely on decays that involve τ leptons, they can also be considered free of NP for the analysis presented here. Nonetheless, the measurements of R_b and γ require a careful discussion in view of existing tensions. Let us therefore start with a detailed discussion of the individual inputs, before proceeding towards a fit of the UT apex.

2.1 The UT Angle γ

The UT angle γ is defined as

$$\gamma \equiv \arg \left(-\frac{V_{ud}V_{ub}^*}{V_{cd}V_{cb}^*} \right), \quad (3)$$

and can be measured in B decays which are sensitive to interference between CKM-favoured $b \rightarrow c$ and CKM-suppressed $b \rightarrow u$ quark-level transitions. The angle γ is determined with high precision from CP violation measurements in $B \rightarrow DK$ decays. The label $B \rightarrow DK$ groups together a long list of decay channels and final states, including $B^+ \rightarrow DK^+$, $B^+ \rightarrow D^*K^+$, $B^+ \rightarrow DK^{*+}$, $B_d^0 \rightarrow DK^{*0}$, $B_s^0 \rightarrow D_s^\mp K^\pm$ and others. Here, D represents an admixture of D^0 and \bar{D}^0 mesons, and similarly for D^* . An overview of the various experimental measurements can be found in Refs. [13,27]. In view of the goal of this paper, to search for NP in B_q -meson mixing, an important distinction needs to be made between the B^+ and B_d^0 decays on the one hand, and the B_s^0 decays on the

other. The sensitivity to γ in the B^+ and B_d^0 decays comes from direct CP violation, which can be measured from decay-time-independent analyses, while the sensitivity to γ in $B_s^0 \rightarrow D_s^\mp K^\pm$ comes from mixing-induced CP violation and requires a decay-time-dependent analysis, taking into account the effects of B_s^0 – \bar{B}_s^0 mixing. This illustrates why we need to be careful when making averages of the different γ measurements.

Decay-time-independent $B \rightarrow DK$ For the decay-time-independent analyses, the latest average from the LHCb collaboration is given by [13]

$$\gamma_{B \rightarrow DK} = (64.9^{+3.9}_{-4.5})^\circ. \quad (4)$$

Since the individual γ measurements could, in principle, be affected by NP effects, it remains important to compare the results from the individual measurements and different decay channels before averaging. NP effects may be washed out in the average, which then also becomes very challenging to interpret theoretically. Here, we will assume that the result (4) is free from NP.

Decay-time-dependent $B_s^0 \rightarrow D_s^\mp K^\pm$ The interpretation of the results from the $B_s^0 \rightarrow D_s^\mp K^\pm$ system requires more attention. Through interference effects with the B_s^0 – \bar{B}_s^0 mixing process, the CP asymmetry parameters in $B_s^0 \rightarrow D_s^\mp K^\pm$ allow a determination of the sum $\phi_s + \gamma$ that is theoretically clean. The latest result for the B_s -meson mixing phase ϕ_s measured in the $B_s^0 \rightarrow J/\psi\phi$ channel and corrected for contributions from penguin topologies [36, 37], is

$$\phi_s = -0.074^{+0.025}_{-0.024} = (-4.2 \pm 1.4)^\circ. \quad (5)$$

With this experimental input, the result for $\phi_s + \gamma$ can be converted into an independent measurement of γ , regardless of possible NP in the B_s^0 – \bar{B}_s^0 mixing phase ϕ_s . Any NP contributions to ϕ_s impact the CP asymmetry measurements in both $B_s^0 \rightarrow J/\psi\phi$ and $B_s^0 \rightarrow D_s^\mp K^\pm$ equally, and thus cancel in the determination of γ . Combining the measured CP asymmetries in $B_s^0 \rightarrow D_s^\mp K^\pm$ [38] with the above value for ϕ_s , gives [19, 20]

$$\gamma_{B_s \rightarrow D_s K} = (131^{+17}_{-22})^\circ, \quad (6)$$

which shows a difference of 3 standard deviations in comparison with the decay-time-independent result of γ in Eq. (4). A dedicated discussion of this result and the puzzling tension with Eq. (4) can be found in Refs. [19, 20]. If this value is to be explained by NP, it requires additional contributions to the $B_s^0 \rightarrow D_s^\mp K^\pm$ decay amplitudes. Remarkably, Refs. [19, 20] have also found puzzling patterns at the branching ratio level, as one would expect with NP effects entering the decay amplitude. What makes the intriguing situation even more exciting, is that consistent patterns are found when complementing the analysis with decays with similar dynamics. In Refs. [19, 20], a model-independent strategy has been presented, showing that the data can be accommodated with NP contributions at the level of 30% of the SM amplitudes. We note that model-dependent studies have also been discussed in Refs. [16–18].

Isospin $B \rightarrow \pi\pi, \rho\pi, \rho\rho$ The UT angle γ can also be determined from an isospin analysis of the decays $B \rightarrow \pi\pi, \rho\pi, \rho\rho$, where B is either B^+ or B_d^0 , and we combine all possible charge combinations for the final states. This method was originally proposed in Ref. [39] for the $B \rightarrow \pi\pi$ system and has been extensively discussed in Ref. [40]. For the remainder of this paper, we will use a shorthand notation and refer to this method as γ from isospin relations, or γ_{iso} . The isospin relations between the $B \rightarrow \pi\pi, \rho\pi, \rho\rho$ decays are exploited to simultaneously control the contributions from penguin topologies affecting these decays, and to determine the weak phase difference

$$\phi_d + 2\gamma = \phi_d^{\text{NP}} - 2\alpha, \quad (7)$$

where

$$\phi_d = \phi_d^{\text{SM}} + \phi_d^{\text{NP}} = 2\beta + \phi_d^{\text{NP}}. \quad (8)$$

In the absence of NP contributions, i.e. $\phi_d^{\text{NP}} = 0$, relation (7) has been used in the literature to interpret the dependence on $\phi_d + 2\gamma$ as an independent measurement of the UT angle α , with the latest result given by [27]

$$\alpha = (85.2^{+4.8}_{-4.3})^\circ. \quad (9)$$

However, ϕ_d^{NP} need not be zero, as we explore in this paper. The isospin analysis therefore does not provide a direct measurement of the CKM angle α , but instead, should be interpreted as an independent measurement of the CKM angle γ , utilising external input on the $B_d^0\text{--}\bar{B}_d^0$ mixing phase ϕ_d . The latest result for ϕ_d , measured in the $B_d^0 \rightarrow J/\psi K^0$ channel and corrected for contributions from penguin topologies, is given as follows [36, 37]:

$$\phi_d = (44.4^{+1.6}_{-1.5})^\circ. \quad (10)$$

It is important to stress that NP effects in $B_d^0\text{--}\bar{B}_d^0$ mixing lead to the same ϕ_d^{NP} contribution in the measurement of ϕ_d from $B_d^0 \rightarrow J/\psi K^0$ and in the determination of the weak phase $\phi_d + 2\gamma$ obtained through the isospin analysis. This NP phase thus cancels when using the experimental input (10), allowing a measurement of γ from $B \rightarrow \pi\pi, \rho\pi, \rho\rho$. Combining the result for $\phi_d + 2\gamma$ in Eq. (9) with the measurement of ϕ_d in Eq. (10), we find

$$\gamma_{\text{iso}} = (72.6^{+4.3}_{-4.9})^\circ. \quad (11)$$

In contrast to the measurement of γ from $B \rightarrow DK$ decays, this value can be affected by possible NP entering the decay amplitudes through penguin topologies.

Average Comparing the values of γ in Eqs. (4) and (11), we find a difference of $(7.5 \pm 6.7)^\circ$. The two γ determinations are consistent within 1.1 standard deviations. Given their different origins, this is a non-trivial result. Since both approaches also have similar precision, there is no preference for one or the other. Because of these two reasons, we have chosen to average the results for our analysis in this paper, and will use

$$\gamma_{\text{avg}} = (68.4 \pm 3.4)^\circ \quad (12)$$

for the fit of the UT apex below. However, it is important to keep in mind that the situation may well change in the future as the measurements of γ become more precise. With improved precision, differences between the approaches could become more pronounced, thereby hinting at NP effects either at the tree-level in $B \rightarrow DK$ decays or at the loop-level in the isospin analysis. If such a situation arises, averaging both results would no longer be justified.

2.2 The UT Side R_b

The second input for the SM fit of the UT apex is the side R_b . It is defined as

$$R_b \equiv \left(1 - \frac{\lambda^2}{2}\right) \frac{1}{\lambda} \left| \frac{V_{ub}}{V_{cb}} \right| = \sqrt{\bar{\rho}^2 + \bar{\eta}^2}. \quad (13)$$

All three CKM matrix elements $\lambda \equiv |V_{us}|$, $|V_{ub}|$ and $|V_{cb}|$ can be measured in semileptonic decays involving electrons or muons, which are generally considered to be robust against NP contributions. Nonetheless, for each of these elements, there are still unresolved discrepancies between the various theoretical and experimental approaches. These discrepancies have a sizable impact on the coordinates of the UT apex, and thus also on the SM predictions and NP searches in B_q -meson mixing. Therefore, even though the tensions have been extensively discussed in the literature (see Ref. [26] for an overview), it is important to summarise them here again.

$|V_{us}|$ The element $|V_{us}|$ is most precisely measured in semileptonic kaon decays. The experimental average from measurements in the $K \rightarrow \pi \ell \nu_\ell$ decay channels, collectively referred to as $K\ell 3$, is [41, 42]

$$|V_{us}| = 0.22309 \pm 0.00056 \quad (\text{from } K\ell 3), \quad (14)$$

while the experimental average from $K \rightarrow \mu \nu_\mu(\gamma)$ decays, referred to as $K\ell 2$, is [26]

$$|V_{us}| = 0.2252 \pm 0.0005 \quad (\text{from } K\ell 2). \quad (15)$$

These two results differ by three standard deviations. The $K\ell 2$ result is derived from the ratio of decay rates

$$\frac{\Gamma(K \rightarrow \mu \nu_\mu(\gamma))}{\Gamma(\pi \rightarrow \mu \nu_\mu(\gamma))} \propto \left(\frac{|V_{us}| f_{K^+}}{|V_{ud}| f_{\pi^+}} \right)^2 \quad (16)$$

between the $K \rightarrow \mu \nu_\mu(\gamma)$ and $\pi \rightarrow \mu \nu_\mu(\gamma)$ decay channels. Here, f_{K^+} and f_{π^+} are the kaon and pion decay constants, respectively, whose ratio is well known from lattice calculations [43]. Furthermore, the measurement of $|V_{us}|$ from Eq. (16) also depends on the CKM matrix element $|V_{ud}|$, whose most precise measurement [26]

$$|V_{ud}| = 0.97373 \pm 0.00031 \quad (17)$$

comes from superallowed nuclear beta decay.

The precise determination of $|V_{ud}|$ offers a third possibility to determine $|V_{us}|$. Using the Wolfenstein parametrisation [24, 25] of the CKM matrix elements

$$|V_{ud}| = 1 - \frac{1}{2}\lambda^2 - \frac{1}{8}\lambda^4 + \mathcal{O}(\lambda^6), \quad |V_{us}| = \lambda + \mathcal{O}(\lambda^7), \quad (18)$$

it is possible to express $|V_{us}|$ in terms of $|V_{ud}|$, resulting in

$$|V_{us}| = 0.2277 \pm 0.0013 \quad (\text{from } |V_{ud}|). \quad (19)$$

Even though the uncertainty on this derived result is much larger than the direct $K\ell 3$ measurement, we again find a difference of 3.3 standard deviations. A comparison with

the $K\ell 2$ measurement is less straightforward as they are not independent results. Alternatively, the measurement of $|V_{us}|$ from $K\ell 3$ predicts a value

$$|V_{ud}| = 0.97481 \pm 0.00013 \quad (\text{from } K\ell 3), \quad (20)$$

which differs from the result (17) by 3.2 standard deviations. A similar tension is found when testing the CKM matrix unitarity relation

$$|V_{ud}|^2 + |V_{us}|^2 + |V_{ub}|^2 = 1. \quad (21)$$

Combining the measurements in Eqs. (17) and (14) with the experimental results for $|V_{ub}|$ introduced below, a difference of 3.2 standard deviations with respect to 1 is found. For this test, the impact of $|V_{ub}|$, which is only proportional to λ^3 , is negligible. Both results suggest that the tension between the $K\ell 3$ and $K\ell 2$ measurements of $|V_{us}|$ may find its origin in a tension between the $|V_{us}|_{K\ell 3}$ and $|V_{ud}|$ measurements.

Lastly, $|V_{us}|$ has also been determined from τ lepton decays. The latest average is [26]

$$|V_{us}| = 0.2221 \pm 0.0013 \quad (\tau \text{ lepton decays}). \quad (22)$$

This result is compatible with the measurement from $K\ell 3$ decays, albeit with a much larger uncertainty, and has a similar precision as the result (19) based on the $|V_{ud}|$ measurement.

Although the tensions between the different determinations of $|V_{us}|$ are intriguing, they turn out to have a negligible impact in the search for NP in B_q -meson mixing. This is illustrated by Fig. 2, which will be discussed in more detail below. Therefore, we will only present the results for the $K\ell 3$ -type decays in the paper, avoiding the dependence on the measurement of $|V_{ud}|$.

$|V_{ub}|$ and $|V_{cb}|$ The CKM matrix elements $|V_{ub}|$ and $|V_{cb}|$ are measured in semileptonic B decays. The latest experimental averages for the inclusive determinations are [27, 44]

$$|V_{ub}|_{\text{incl}} = (4.19 \pm 0.17) \times 10^{-3}, \quad |V_{cb}|_{\text{incl}} = (42.16 \pm 0.50) \times 10^{-3}, \quad (23)$$

where $|V_{ub}|$ is calculated using the Gambino–Giordano–Ossola–Uraltsev (GGOU) [45] approach, while the determination of $|V_{cb}|$ uses the kinematic scheme and includes the latest three-loop calculations of the total semileptonic width [44]. These results, however, differ by respectively 3.9 and 4.3 standard deviations from the exclusive determinations from the Heavy Flavour Averaging Group (HFLAV) [27]

$$|V_{ub}|_{\text{excl}} = (3.51 \pm 0.12) \times 10^{-3}, \quad |V_{cb}|_{\text{excl}} = (39.10 \pm 0.50) \times 10^{-3}, \quad (24)$$

which include constraints on the ratio $|V_{ub}|/|V_{cb}|$ from LHCb measurements of the decays $\Lambda_b^0 \rightarrow p\mu^-\bar{\nu}_\mu$ [46] and $B_s^0 \rightarrow K^-\mu^+\nu_\mu$ [47]. Contrary to the situation for $|V_{us}|$, these differences do have a significant impact on the analysis presented in this paper, and lead to different pictures for the allowed parameter spaces for NP in B_q -meson mixing. Therefore, we will explicitly show all results for both the inclusive and the exclusive determinations. This illustrates the importance of further investigating the origin of these tensions and of eventually resolving them.

R_b Combining the measurements of $|V_{us}|$, $|V_{ub}|$ and $|V_{cb}|$, we can calculate the UT side R_b . Due to the unresolved discrepancies between the different determinations of these CKM matrix elements, the numerical value for R_b will strongly depend on our choices for the individual inputs. The two most common combinations found in the literature pair the inclusive (or exclusive) determinations of $|V_{ub}|$ and $|V_{cb}|$ with each other, resulting in a fully inclusive (or exclusive) value for R_b :

$$R_{b,\text{incl},K\ell 3} = 0.434 \pm 0.018, \quad R_{b,\text{excl},K\ell 3} = 0.392 \pm 0.014. \quad (25)$$

These two values differ from each other by 2.4 standard deviations. Recent discussions in the literature [10, 44, 48, 49], aiming to understand and resolve the tension between the inclusive and exclusive values of $|V_{ub}|$ and $|V_{cb}|$, have sparked interest in a third possibility: The hybrid combination of the exclusive value for $|V_{ub}|$ with the inclusive value for $|V_{cb}|$. This results in a value for R_b of

$$R_{b,\text{hybrid},K\ell 3} = 0.364 \pm 0.013, \quad (26)$$

which differs from the inclusive (exclusive) R_b solution by 3.7 (1.5) standard deviations. In this paper we will consider all three options to illustrate the impact that the numerical values of $|V_{ub}|$ and $|V_{cb}|$ have on our searches for beyond the SM physics.

2.3 The UT Apex

The coordinates $(\bar{\rho}, \bar{\eta})$ of the UT apex are determined from a fit to R_b and γ , based on the numerical inputs summarised in Table 1. The fitting procedure is implemented using the GammaCombo framework [50], and gives the following results:

$$\text{Incl, } K\ell 3 \quad \bar{\rho} = 0.160 \pm 0.025, \quad \bar{\eta} = 0.404 \pm 0.022, \quad (27)$$

$$\text{Excl, } K\ell 3 \quad \bar{\rho} = 0.144 \pm 0.022, \quad \bar{\eta} = 0.365 \pm 0.018, \quad (28)$$

$$\text{Hybrid, } K\ell 3 \quad \bar{\rho} = 0.134 \pm 0.021, \quad \bar{\eta} = 0.338 \pm 0.017, \quad (29)$$

with the associated two-dimensional confidence level contours shown in Fig. 1. The three solutions for the UT apex are compared with one other in Fig. 2.

The impact of the different measurements of $|V_{us}|$ and γ on the UT apex is illustrated in Fig. 2, taking the exclusive scenario as an example. At present, all results agree within uncertainties, but with improved precision, this may no longer be the case in the future. We will explore this further in Section 6.

2.4 Comparison with $|\varepsilon_K|$

The apex of the UT is not only constrained by information from B -meson physics, but also by other flavour processes. CP violation in the neutral kaon system constrains the UT apex through the observable $|\varepsilon_K|$. In the SM, the dependence of $|\varepsilon_K|$ on the UT apex coordinates $\bar{\rho}$ and $\bar{\eta}$ is given by [51]:

$$|\varepsilon_K| = \frac{G_F^2 m_W^2 m_K f_K^2}{6\sqrt{2}\pi^2 \Delta m_K} \kappa_\varepsilon \hat{B}_K |V_{cb}|^2 \lambda^2 \bar{\eta} \left[|V_{cb}|^2 (1 - \bar{\rho}) \eta_{tt}^{\text{EW}} \eta_{tt} \mathcal{S}(x_t) - \eta_{ut} \mathcal{S}(x_c, x_t) \right], \quad (30)$$

where G_F is the Fermi constant, m_W and m_K are the W and kaon mass, respectively, f_K is the kaon decay constant, Δm_K is the mass difference between the K_S^0 and K_L^0 mass

	Inclusive	Exclusive	Hybrid	Reference
α		$(85.2^{+4.8}_{-4.3})^\circ$		[27]
ϕ_d		$(44.4^{+1.6}_{-1.5})^\circ$		[36, 37]
$\gamma_{B \rightarrow DK}$		$(64.9^{+3.9}_{-4.5})^\circ$		[13]
γ_{iso}		$(72.6^{+4.3}_{-4.9})^\circ$		-
γ_{avg}		$(68.4 \pm 3.3)^\circ$		-
$ V_{us} $	0.22309 ± 0.00056			[26]
$ V_{ub} \times 10^3$	4.19 ± 0.17	3.51 ± 0.12	3.51 ± 0.12	[27]
$ V_{cb} \times 10^3$	42.16 ± 0.50	39.10 ± 0.50	42.16 ± 0.50	[27, 44]
R_b	0.434 ± 0.018	0.392 ± 0.014	0.364 ± 0.013	-
$\bar{\rho}$	0.160 ± 0.025	0.144 ± 0.022	0.134 ± 0.021	-
$\bar{\eta}$	0.404 ± 0.022	0.365 ± 0.018	0.338 ± 0.017	-

Table 1: Input parameters and results for the determination of the UT apex, split between the inclusive, exclusive and hybrid determinations of R_b . The dashes in the reference column indicate derived quantities that were computed in this paper.

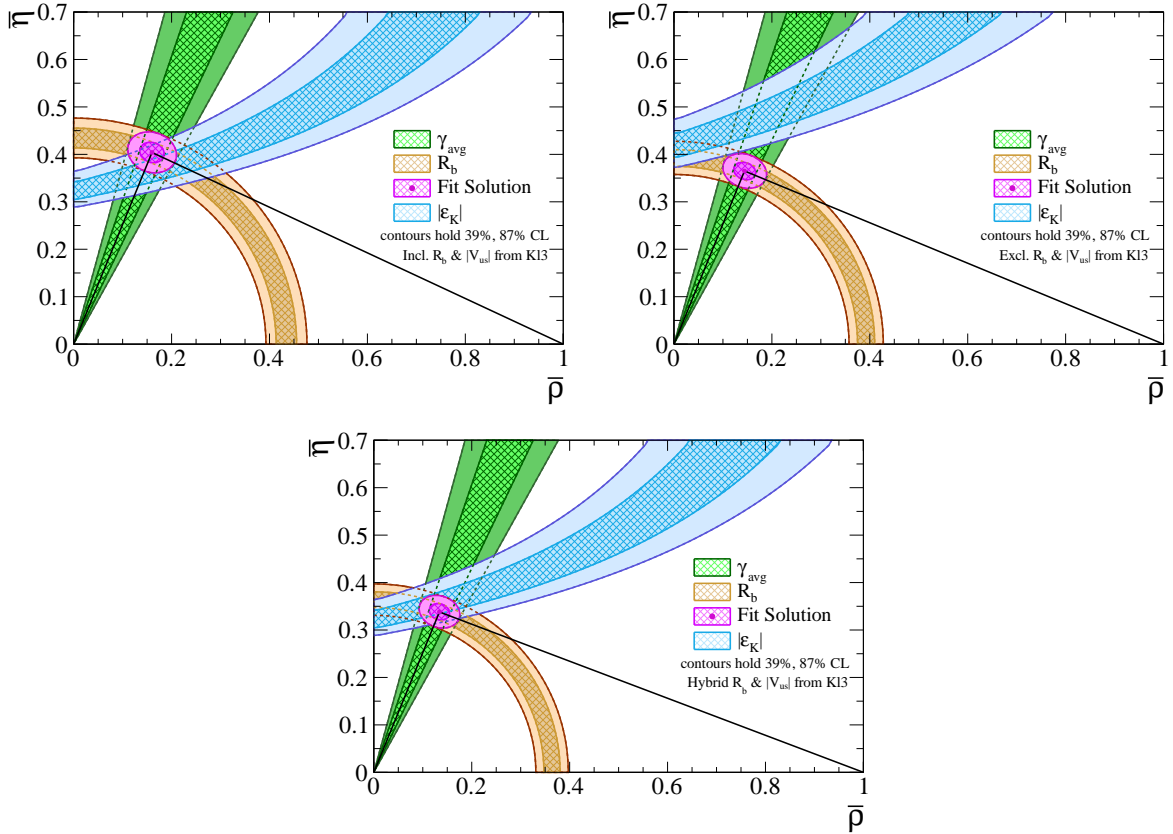


Figure 1: Determination of the coordinates $(\bar{\rho}, \bar{\eta})$ of the UT apex from measurements of the angle γ and the side R_b , with the two-dimensional confidence level contours from the GammaCombo fit overlaid. For comparison, the constraint from $|\varepsilon_K|$, discussed in Section 2.4, is shown (but not included in the fit). The solutions based on the inclusive (Left), exclusive (Right) and hybrid (Bottom) determination of R_b are shown separately.

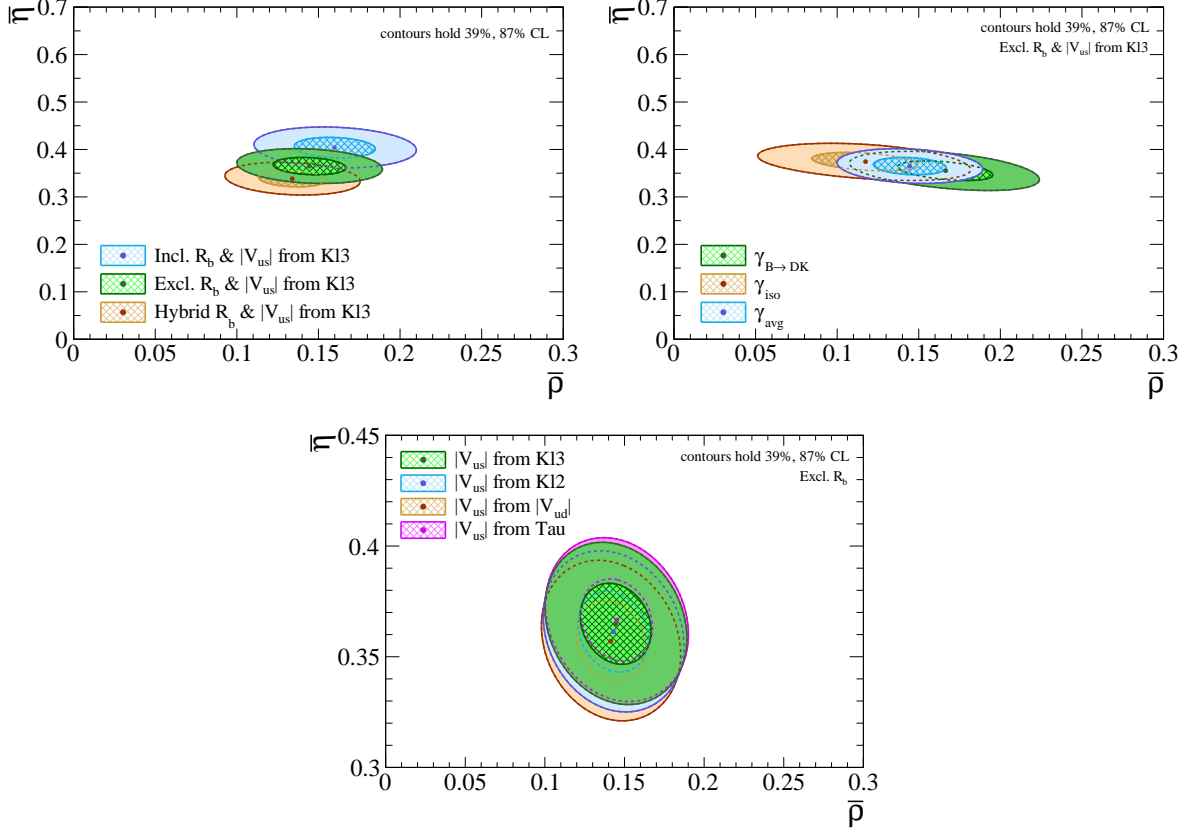


Figure 2: Two-dimensional confidence level contours for the coordinates $(\bar{\rho}, \bar{\eta})$ of the UT apex. Left: Comparison between the inclusive, exclusive and hybrid scenarios. Right: Comparison between the different values for the angle γ in the exclusive scenario. Bottom: Comparison between different values for $|V_{us}|$ in the exclusive scenario.

eigenstates, and \hat{B}_K is the kaon bag parameter. The parameter κ_ε is a multiplicative correction factor [52] due to long-distance contributions that are not included in \hat{B}_K . The functions

$$\mathcal{S}(x_t) = S_0(x_t) + S_0(x_c) - 2S_0(x_c, x_t), \quad \mathcal{S}(x_c, x_t) = S_0(x_c) - S_0(x_c, x_t) \quad (31)$$

are combinations of the following two Inami–Lim functions [53]:

$$S_0(x_i) = x_i \left[\frac{1}{4} + \frac{9}{4(1-x_i)} - \frac{3}{2(1-x_i)^2} - \frac{3x_i^2 \ln x_i}{2(1-x_i)^3} \right], \quad (32)$$

$$S_0(x_i, x_j) = \frac{x_i x_j}{x_i - x_j} \left[\frac{1}{4} + \frac{3}{2(1-x_i)} - \frac{3}{4(1-x_i)^2} \right] \ln x_i \quad (33)$$

$$+ \frac{x_j x_i}{x_j - x_i} \left[\frac{1}{4} + \frac{3}{2(1-x_j)} - \frac{3}{4(1-x_j)^2} \right] \ln x_j - \frac{3x_i x_j}{4(1-x_i)(1-x_j)}, \quad (34)$$

where

$$x_i \equiv \left[\frac{\bar{m}_i(\bar{m}_i)}{m_W} \right]^2 \quad \text{with } i = c, t, \quad (35)$$

	Value	Unit	Reference
G_F	$1.1663787 \times 10^{-11}$	MeV^{-2}	[26]
m_W	$80\,377 \pm 12$	MeV	[26] [†]
m_K	497.611 ± 0.013	MeV	[26]
$\bar{m}_c(\bar{m}_c)$	1.278 ± 0.013	GeV	[43]
m_t	172.69 ± 0.30	GeV	[26]
m_Z	91.1876 ± 0.0021	GeV	[26]
$\alpha_s(m_Z)$	0.1179 ± 0.0009		[26]
$\bar{m}_t(\bar{m}_t)$	162.19 ± 0.30	GeV	-
Δm_K	0.005289 ± 0.000010	ps^{-1}	[26]
f_K	155.7 ± 0.3	MeV	[43]
\hat{B}_K	0.7625 ± 0.0097		[43]
κ_ε	0.94 ± 0.02		[52]
η_{tt}^{EW}	0.990 ± 0.004		[56]
η_{tt}	0.550 ± 0.023		[51]
η_{ut}	0.402 ± 0.005		[51] [‡]

	Inclusive & Hybrid	Exclusive	Unit	Reference
A	$(6.94 \pm 0.40) \times 10^{-3}$	$(5.36 \pm 0.32) \times 10^{-3}$		-
B	$(5.11 \pm 0.35) \times 10^{-3}$	$(3.78 \pm 0.27) \times 10^{-3}$		-
$ \varepsilon_K _{\text{SM}}$	$(2.54 \pm 0.22) \times 10^{-3}$	$(1.74 \pm 0.15) \times 10^{-3}$		-
$ \varepsilon_K _{\text{exp}}$	$(2.228 \pm 0.011) \times 10^{-3}$			[26]

Table 2: Input parameters and results for the SM calculation of $|\varepsilon_K|$, split between the inclusive and exclusive determinations of $|V_{cb}|$. The dashes in the reference column indicate derived quantities computed in this paper. [†] This average does not yet include the new measurement from the CDF II experiment [57], but the difference with the current world average has no significant impact on the numerical prediction for $|\varepsilon_K|_{\text{SM}}$. [‡] Ref. [58] has computed a correction factor for η_{ut} of 1.005, which is not yet included here but has a negligible impact on $|\varepsilon_K|$.

and $\bar{m}_i(\bar{m}_i)$ is the mass of quark i in the $\overline{\text{MS}}$ scheme. For the top quark, we use the RunDec tool [54, 55] to convert the latest experimental average of the pole mass [26] into

$$\bar{m}_t(\bar{m}_t) = (162.19 \pm 0.30) \text{ GeV} , \quad (36)$$

ignoring light-quark mass effects and using additional experimental input for the Z boson mass m_Z and the QCD coupling constant $\alpha_s(m_Z)$. Finally, η_{tt}^{EW} , η_{tt} and η_{ut} are correction factors to the modified Inami–Lim functions $\mathcal{S}(x_t)$ and $\mathcal{S}(x_c, x_t)$ due to next-to-leading order (NLO) electroweak and QCD contributions [51, 56]. The factors η_{tt} and η_{ut} parametrise the QCD corrections and are known to next-to-leading-logarithmic (NLL) and next-next-to-leading-logarithmic (NNLL) precision, respectively [51]. The factor η_{tt}^{EW} estimates the impact of NLO electroweak corrections based on the first calculations of two-loop electroweak contributions to ε_K [56]. All numerical values for the observables in Eq. (30) are listed in Table 2.

As can be seen from Eq. (30), the CP-violating observable $|\varepsilon_K|$ depends on both the

square and fourth power of $|V_{cb}|$ and is thus highly sensitive to its numerical value. With sufficient precision, $|\varepsilon_K|$ could therefore be an excellent observable to explore the tension between the inclusive and exclusive determinations of $|V_{cb}|$, as it might favour one of the two. If the tension between both determinations is resolved in the future, a discrepancy between the constraint coming from $|\varepsilon_K|$ and the fit results for the UT apex could point to NP in neutral kaon mixing.

In the SM, the measured value of $|\varepsilon_K|$ describes a hyperbola

$$\bar{\eta} = \frac{|\varepsilon_K|}{A - B\bar{\rho}} \quad (37)$$

in the $\bar{\rho} - \bar{\eta}$ plane. Using our solutions for the UT apex in Eqs. (27)–(29), we find the SM predictions

$$\text{Incl, } K\ell 3 \quad |\varepsilon_K|_{\text{SM}} = (2.54 \pm 0.22) \times 10^{-3}, \quad (38)$$

$$\text{Excl, } K\ell 3 \quad |\varepsilon_K|_{\text{SM}} = (1.74 \pm 0.15) \times 10^{-3}, \quad (39)$$

where the inclusive value also covers the hybrid scenario, as $|\varepsilon_K|_{\text{SM}}$ only depends on $|V_{cb}|$. The values of A and B can be found in Table 2. The differences between the SM predictions and the experimental result [26]

$$|\varepsilon_K| = (2.228 \pm 0.011) \times 10^{-3} \quad (40)$$

are 1.4 and 3.2 standard deviations for the inclusive/hybrid and exclusive scenarios, respectively. This shows a preference for the inclusive value, but the uncertainty on the SM predictions is not yet sufficient to draw any further conclusions.

The same conclusion also arises from the comparison between the contours following from the measurement of $|\varepsilon_K|$ and the fit solution for the UT apex fixed through γ and R_b , shown in Fig. 1. Besides finding the same small tensions as between Eqs. (38), (39) and (40), it is interesting that the contour for $|\varepsilon_K|$ from the exclusive determination lies completely above the fit solution from γ and R_b , while the contour from the inclusive determination lies mainly below the corresponding fit solution. The contour from the hybrid determination falls in between the inclusive and exclusive determinations, and overlaps with the fit solution. Out of the three scenarios, it gives the most consistent picture of the UT apex. This illustrates the strong dependence on the value of $|V_{cb}|$, which in the future could help to understand the puzzle between the inclusive and exclusive scenarios, assuming NP in kaon mixing can be controlled or ignored.

3 $B_q^0 - \bar{B}_q^0$ Mixing in the Standard Model

In the SM, mixing between the neutral B_q^0 and \bar{B}_q^0 mesons originates from box diagrams. Since these are loop processes and thus strongly suppressed, the mixing phenomenon is an excellent place for NP to enter. The determination of the parameter space of possible NP contributions to $B_q^0 - \bar{B}_q^0$ mixing will rely on the results for the UT apex from Section 2.3, which are needed to compute the SM predictions of the mixing parameters characterising neutral B_q -meson mixing. Comparing their SM predictions to the corresponding experimental values will allow us to constrain possible NP effects in $B_q^0 - \bar{B}_q^0$ mixing, as we will show in Section 4.

3.1 The Mixing Parameters in the Standard Model

The SM prediction of the mixing angle ϕ_d is given by:

$$\phi_d^{\text{SM}} = 2\beta = 2\arg\left(-\frac{V_{cd}V_{cb}^*}{V_{td}V_{tb}^*}\right) = 2\tan^{-1}\left(\frac{\bar{\eta}}{1-\bar{\rho}}\right). \quad (41)$$

Using Eqs. (27)–(29), we obtain the following results:

$$\text{Incl, } K\ell 3 \quad \phi_d^{\text{SM}} = (51.4 \pm 2.8)^\circ, \quad (42)$$

$$\text{Excl, } K\ell 3 \quad \phi_d^{\text{SM}} = (46.2 \pm 2.3)^\circ, \quad (43)$$

$$\text{Hybrid, } K\ell 3 \quad \phi_d^{\text{SM}} = (42.6 \pm 2.2)^\circ. \quad (44)$$

These can be compared to the experimental measurement of ϕ_d that was already given in Eq. (10).

The SM expression for ϕ_s is given by:

$$\phi_s^{\text{SM}} = -2\delta\gamma = -2\lambda^2\bar{\eta} + \mathcal{O}(\lambda^4), \quad (45)$$

which at this order in the Wolfenstein parametrisation [24, 25] can be expressed in terms of either η or $\bar{\eta}$ interchangeably. Note that in contrast to the expression for ϕ_d^{SM} , the dependence on the UT apex is doubly Cabibbo-suppressed. The numerical predictions based on Eqs. (27)–(29) are:

$$\text{Incl, } K\ell 3 \quad \phi_s^{\text{SM}} = -0.0402 \pm 0.0022 = (-2.30 \pm 0.13)^\circ, \quad (46)$$

$$\text{Excl, } K\ell 3 \quad \phi_s^{\text{SM}} = -0.0363 \pm 0.0018 = (-2.08 \pm 0.10)^\circ, \quad (47)$$

$$\text{Hybrid, } K\ell 3 \quad \phi_s^{\text{SM}} = -0.0336 \pm 0.0017 = (-1.93 \pm 0.10)^\circ. \quad (48)$$

These SM predictions are a factor 2.5 to 3 less precise than the value [11]

$$\phi_s^{\text{SM}} = -0.03682_{-0.00060}^{+0.00086} = (-2.110_{-0.034}^{+0.049})^\circ, \quad (49)$$

which was obtained from a global fit of the UT, and is commonly referenced in the literature. However, the global UT fits rely for their input on information from $B_q^0\text{--}\bar{B}_q^0$ mixing, without accounting for possible contributions from NP that may introduce biases. We will therefore not use these results here and trade the loss in precision for a better control of the possible NP effects that could enter this determination. The experimental measurement of ϕ_s is given in Eq. (5).

The mass difference between the heavy and light mass eigenstates of the neutral B_q -meson system is given by

$$\Delta m_q = 2|M_{12}^q| + \mathcal{O}\left(\left|\frac{\Gamma_{12}^q}{M_{12}^q}\right|^2\right), \quad (50)$$

where $M_{12}^q - \frac{i}{2}\Gamma_{12}^q$ is the off-diagonal element of the effective Hamiltonian describing $B_q^0\text{--}\bar{B}_q^0$ mixing. In the SM, the element M_{12}^q is given as

$$|M_{12}^q|_{\text{SM}} = \frac{G_F^2 m_W^2}{12\pi^2} m_{B_q} |V_{tq}V_{tb}|^2 S_0(x_t) \eta_{2B} \hat{B}_{B_q} f_{B_q}^2, \quad (51)$$

	Inclusive	Exclusive	Hybrid	Unit	Reference
m_{B_s}		5366.92 ± 0.10		MeV	[26]
m_{B_d}		5279.66 ± 0.12		MeV	[26]
$f_{B_d} \sqrt{\hat{B}_{B_d}}$		210.6 ± 5.5		MeV	[61]
$f_{B_s} \sqrt{\hat{B}_{B_s}}$		256.1 ± 5.7		MeV	[61]
ξ		1.212 ± 0.016			[61]
Δm_d^{SM}	0.513 ± 0.040	0.439 ± 0.033	0.510 ± 0.037	ps^{-1}	-
Δm_s^{SM}	17.23 ± 0.87	14.80 ± 0.76	17.19 ± 0.87	ps^{-1}	-
Δm_d		0.5065 ± 0.0019		ps^{-1}	[27]
Δm_s		17.7656 ± 0.0057		ps^{-1}	[27, 63]
ϕ_d^{SM}	51.4 ± 2.8	46.2 ± 2.3	42.6 ± 2.2	Degrees	-
ϕ_s^{SM}	-2.30 ± 0.13	-2.08 ± 0.10	-1.93 ± 0.10	Degrees	-
ϕ_d		$44.4^{+1.6}_{-1.5}$		Degrees	[36, 37]
ϕ_d		-4.2 ± 1.4		Degrees	[36, 37]

Table 3: Input values and results for the determination of the $B_q^0\text{--}\bar{B}_q^0$ mixing parameters Δm_q and ϕ_q . The dashes in the reference column indicate derived quantities that were computed in this paper.

where m_{B_q} is the B_q mass, f_{B_q} is the B_q decay constant, \hat{B}_{B_q} is the renormalisation group invariant bag parameter, $S_0(x_t)$ is the Inami–Lim function given in Eq. (32), and $\eta_{2B} = 0.551$ is a short-distance QCD correction factor [59, 60]. The decay constants and bag parameters have been calculated using lattice QCD methods. The latest computation using $N_f = 2 + 1 + 1$ quark flavours gives the following results [43, 61]:

$$f_{B_d} \sqrt{\hat{B}_{B_d}} = (210.6 \pm 5.5) \text{ MeV} , \quad f_{B_s} \sqrt{\hat{B}_{B_s}} = (256.1 \pm 5.7) \text{ MeV} . \quad (52)$$

The uncertainty on η_{2B} is $\mathcal{O}(1\%)$ [60], and can therefore still be neglected with the current precision. Eq. (51) does not take into account next-to-leading-order electroweak effects, which have been calculated in Ref. [62] to be at the level of 1%. Hence, they can also be omitted given the current precision. The values of all parameters needed to compute Δm_q^{SM} are summarised in Table 3.

Using the Wolfenstein parametrisation of the CKM matrix [24, 25], we can rewrite the CKM matrix elements appearing in the SM expression for the mass differences Δm_q in terms of the experimental inputs and the coordinates of the UT apex that were discussed in Section 2:

$$|V_{td}V_{tb}| = \lambda|V_{cb}|\sqrt{(1 - \bar{\rho})^2 + \bar{\eta}^2} + \mathcal{O}(\lambda^7) , \quad (53)$$

$$= \lambda|V_{cb}|\sqrt{1 - 2R_b \cos \gamma + R_b^2} + \mathcal{O}(\lambda^7) , \quad (54)$$

$$|V_{ts}V_{tb}| = |V_{cb}| \left[1 - \frac{\lambda^2}{2} (1 - 2\bar{\rho}) \right] + \mathcal{O}(\lambda^6) , \quad (55)$$

$$= |V_{cb}| \left[1 - \frac{\lambda^2}{2} (1 - 2R_b \cos \gamma) \right] + \mathcal{O}(\lambda^6) . \quad (56)$$

We see that $|V_{td}V_{tb}|$, and thus Δm_d^{SM} , depends at leading order on $\bar{\rho}$ and $\bar{\eta}$, while for $|V_{ts}V_{tb}|$ and Δm_s^{SM} the dependence on the UT apex only enters at next-to-leading order

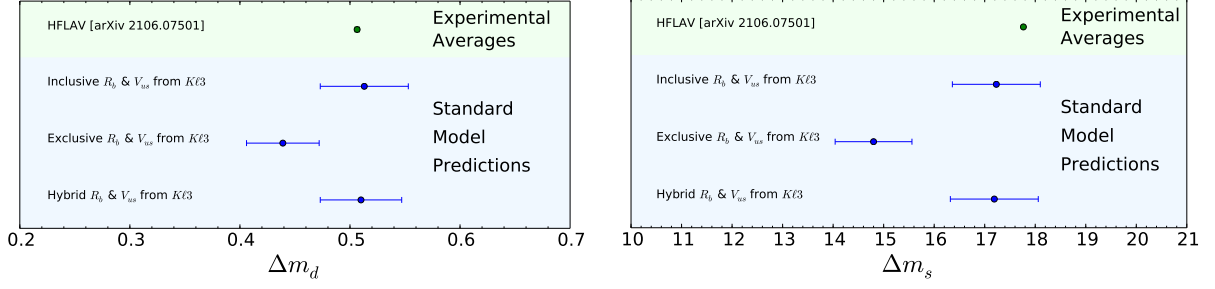


Figure 3: Comparison of the experimental averages and SM predictions for the $B_q^0\text{--}\bar{B}_q^0$ mixing parameters Δm_d (Left) and Δm_s (Right).

in λ . In these expressions, the difference between ρ and $\bar{\rho}$ is of the same order as the neglected terms.

We find the following predictions for the mass differences Δm_q :

$$\text{Incl, } K\ell 3 \quad \Delta m_d^{\text{SM}} = (0.513 \pm 0.040) \text{ ps}^{-1}, \quad \Delta m_s^{\text{SM}} = (17.23 \pm 0.87) \text{ ps}^{-1}, \quad (57)$$

$$\text{Excl, } K\ell 3 \quad \Delta m_d^{\text{SM}} = (0.439 \pm 0.033) \text{ ps}^{-1}, \quad \Delta m_s^{\text{SM}} = (14.80 \pm 0.76) \text{ ps}^{-1}, \quad (58)$$

$$\text{Hybrid, } K\ell 3 \quad \Delta m_d^{\text{SM}} = (0.510 \pm 0.037) \text{ ps}^{-1}, \quad \Delta m_s^{\text{SM}} = (17.19 \pm 0.87) \text{ ps}^{-1}. \quad (59)$$

These SM predictions can be compared with the experimental measurements [27, 63]:

$$\Delta m_d = (0.5065 \pm 0.0019) \text{ ps}^{-1}, \quad (60)$$

$$\Delta m_s = (17.7656 \pm 0.0057) \text{ ps}^{-1}, \quad (61)$$

which are already one to two orders of magnitude more precise. Similar results have been obtained from a combined analysis of lattice and light-cone QCD sum rules (LQSR) results in Ref. [64]. The experimental values and the SM predictions can be visually compared with each other as in Fig. 3, or numerically through the ratio

$$\rho_q \equiv \frac{\Delta m_q}{\Delta m_q^{\text{SM}}}, \quad (62)$$

which equals 1 in the SM. With the results in Eqs. (57)–(61), we obtain:

$$\text{Incl, } K\ell 3 \quad \rho_d = 0.989 \pm 0.078, \quad \rho_s = 1.031 \pm 0.052, \quad (63)$$

$$\text{Excl, } K\ell 3 \quad \rho_d = 1.153 \pm 0.088, \quad \rho_s = 1.200 \pm 0.062, \quad (64)$$

$$\text{Hybrid, } K\ell 3 \quad \rho_d = 0.993 \pm 0.073, \quad \rho_s = 1.034 \pm 0.052. \quad (65)$$

For the inclusive and hybrid scenarios, the ratios are compatible with 1, and thus the SM, while those from the exclusive scenario differ by (15–20)%. In the exclusive scenario, the SM predictions for Δm_s and Δm_d differ by respectively 3 and 2 standard deviations from their experimentally measured values. The smaller central values for Δm_s^{SM} and Δm_d^{SM} in the exclusive scenario compared to the inclusive and hybrid scenarios, and hence the smaller discrepancies with the experimental measurements, are due to the value of $|V_{cb}|$, which shows the same pattern.

3.2 Determining the UT Apex from R_b and Mixing

If we assume the SM expressions for the $B_q^0\text{--}\bar{B}_q^0$ mixing parameters Δm_d and Δm_s , it is possible to determine the UT apex without having to rely on information from γ . Although this scenario is not considered as the baseline, due to the strong assumption that needs to be made, it can be a useful alternative when discrepancies arise between the various measurements of γ . It is therefore interesting to explore this option as well.

In the scenario without γ , the coordinates of the UT apex are fixed by the values of the sides R_b and R_t . The UT side R_t is defined as

$$R_t \equiv \left| \frac{V_{td}V_{tb}}{V_{cd}V_{cb}} \right| = \sqrt{(1 - \bar{\rho})^2 + \bar{\eta}^2} = \frac{1}{\lambda} \left| \frac{V_{td}}{V_{ts}} \right| \left[1 - \frac{\lambda^2}{2} (1 - 2\bar{\rho}) \right] + \mathcal{O}(\lambda^4) , \quad (66)$$

where the ratio of CKM matrix elements

$$\left| \frac{V_{td}}{V_{ts}} \right| = \xi \sqrt{\frac{m_{B_s} \Delta m_d^{\text{SM}}}{m_{B_d} \Delta m_s^{\text{SM}}}} \quad (67)$$

can be determined from the $B_q^0\text{--}\bar{B}_q^0$ mixing parameters. Here,

$$\xi \equiv \frac{f_{B_s} \sqrt{\hat{B}_{B_s}}}{f_{B_d} \sqrt{\hat{B}_{B_d}}} \quad (68)$$

is the ratio of bag parameters and decay constants of the B_d and the B_s systems. This ratio has been calculated on the lattice, with the latest value given by [43, 61]:

$$\xi = 1.212 \pm 0.016 . \quad (69)$$

Compared to the individual results for the bag parameters and decay constants in Table 3, it is known with much higher precision as many uncertainties cancel in the ratio. Combining this result with the experimental values of Δm_d and Δm_s in Eqs. (60) and (61) we get

$$\left| \frac{V_{td}}{V_{ts}} \right| = 0.2063 \pm 0.0004 \pm 0.0027 , \quad (70)$$

where the first uncertainty is due to the experimental measurements and the second due to the lattice input.

The coordinates of the UT apex, determined from a fit to the sides R_b and R_t are

$$\text{Incl, } K\ell 3 \quad \bar{\rho} = 0.180 \pm 0.014 , \quad \bar{\eta} = 0.395 \pm 0.020 , \quad (71)$$

$$\text{Excl, } K\ell 3 \quad \bar{\rho} = 0.163 \pm 0.013 , \quad \bar{\eta} = 0.357 \pm 0.017 , \quad (72)$$

$$\text{Hybrid, } K\ell 3 \quad \bar{\rho} = 0.153 \pm 0.013 , \quad \bar{\eta} = 0.330 \pm 0.016 , \quad (73)$$

with the two-dimensional confidence level contours shown in Fig. 5. Compared to the fit results based on R_b and γ in Eqs. (27)–(29), we find a similar precision for $\bar{\eta}$, while the precision on $\bar{\rho}$ is a factor 2 better. The solutions (71)–(73) correspond to the values

$$\text{Incl, } K\ell 3 \quad R_t = 0.910 \pm 0.012 , \quad (74)$$

$$\text{Excl, } K\ell 3 \quad R_t = 0.909 \pm 0.012 , \quad (75)$$

$$\text{Hybrid, } K\ell 3 \quad R_t = 0.909 \pm 0.012 , \quad (76)$$

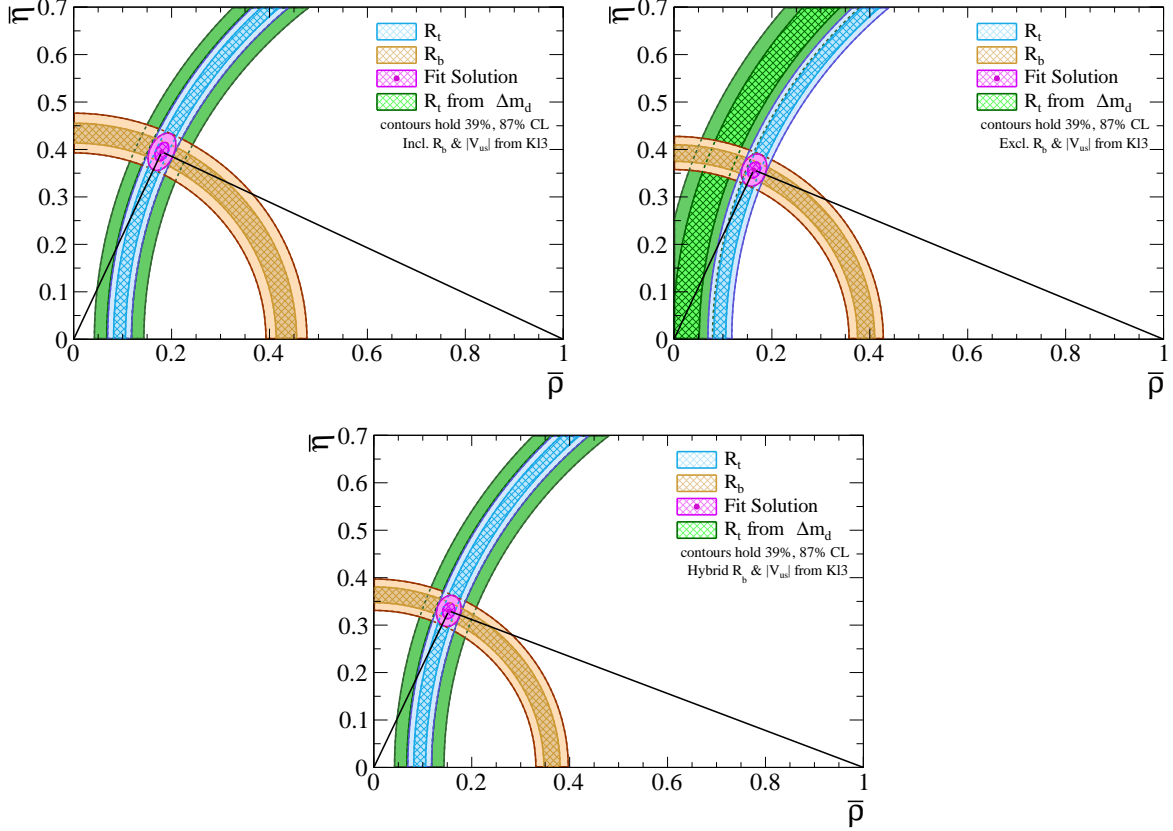


Figure 4: Determination of the UT apex $(\bar{\rho}, \bar{\eta})$ from the measurements of the sides R_b and R_t . For comparison, also the constraint from Δm_d alone is shown (but not included in the fit). The solutions based on the inclusive (Left), exclusive (Right) and hybrid (Bottom) determination of R_b are shown separately.

which can be compared to the values for R_t calculated from Eqs. (27)–(29):

$$\text{Incl, } K\ell 3 \quad R_t = 0.932 \pm 0.024, \quad (77)$$

$$\text{Excl, } K\ell 3 \quad R_t = 0.930 \pm 0.021, \quad (78)$$

$$\text{Hybrid, } K\ell 3 \quad R_t = 0.930 \pm 0.021. \quad (79)$$

Also here the scenarios with γ are a factor 2 less precise than the scenarios without γ .

Alternatively, R_t can also be determined without relying on information from the B_s system, which has the advantage that its value will not be affected by NP in $B_s^0\text{--}\bar{B}_s^0$ mixing. The comparison with the results in Eqs. (74)–(76) then theoretically provides another way to constrain NP effects in the B_s -meson system. The disadvantage of this approach is that we cannot use the ratio ξ of bag parameters and decay constants, which will result in larger associated uncertainties. In this alternative method, R_t is calculated from the definition in Eq. (66), using the inclusive or exclusive value of $|V_{cb}|$, and obtaining $|V_{td}V_{tb}|$ from the measurement of Δm_d through Eq. (51). The approach using only the measurement of Δm_d , and avoiding Δm_s , gives

$$\text{Incl, } K\ell 3 \quad R_t = 0.926 \pm 0.027, \quad (80)$$

$$\text{Excl, } K\ell 3 \quad R_t = 0.999 \pm 0.029, \quad (81)$$

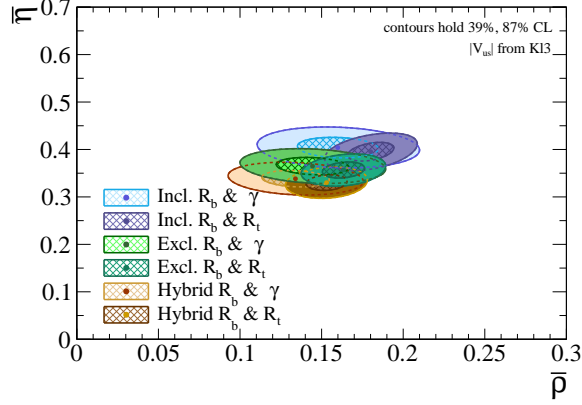


Figure 5: Comparison of the two-dimensional confidence regions for the UT apex $(\bar{\rho}, \bar{\eta})$ determined through γ and R_b , and through R_b and R_t .

with the hybrid scenario matching the inclusive result as it does not depend on $|V_{ub}|$. The corresponding contour is also shown in Fig. 4. Given the current precision, the results for R_t determined through only Δm_d are not competitive with the results for R_t determined through ξ . Hence, we will only use R_t determined through ξ in our analysis. For the inclusive and hybrid scenarios the two determinations of R_t overlap completely, while a slight discrepancy is visible for the exclusive scenario. Combined with the relatively large errors on R_t determined through Δm_d , it does not yet allow us to draw any conclusions regarding NP in B_s mixing.

From the comparison in Fig. 5, we can see that the determination of the apex from R_b and R_t is more precise than the one utilising R_b and γ . However, R_t has been determined assuming SM expressions for Δm_d and Δm_s , and hence ignores contributions from possible NP in $B_q^0-\bar{B}_q^0$ mixing. Possible NP will contaminate the determination of R_t , except in the special case of FUNP. In such scenarios, possible NP in $B_q^0-\bar{B}_q^0$ mixing drops out in the ratio between Δm_d and Δm_s . To determine NP in $B_q^0-\bar{B}_q^0$ mixing in a general scenario, we cannot use the above determination of R_t , but we need the UT apex determination of R_b and γ discussed in Section 2.3. In the next Section we will investigate in more detail what impact the different determinations of the UT apex have on NP searches in $B_q^0-\bar{B}_q^0$ mixing.

4 New Physics in $B_q^0-\bar{B}_q^0$ Mixing

We can use the SM predictions for the mixing parameters Δm_q and ϕ_q , together with their experimental values, to constrain the parameter space of possible NP in $B_q^0-\bar{B}_q^0$ mixing. We introduce the NP parameters κ_q and σ_q by modifying the mixing parameters in the same way as in Ref. [1]:

$$\Delta m_q = \Delta m_q^{\text{SM}} (1 + \kappa_q e^{i\sigma_q}) , \quad (82)$$

$$\phi_q = \phi_q^{\text{SM}} + \phi_q^{\text{NP}} = \phi_q^{\text{SM}} + \arg(1 + \kappa_q e^{i\sigma_q}) . \quad (83)$$

Here, the size of the NP effects is described by κ_q , while σ_q is a complex phase that accounts for additional CP-violating effects. This parametrisation is model-independent;

	Scenario I	Scenario II	Scenario III
Assumptions	no NP in γ	FUNP	partial FUNP
UT apex fit	R_b and γ	R_b and R_t	R_b and R_t
NP parameters	(κ_d, σ_d) and (κ_s, σ_s)	$(\kappa_d, \sigma_d) = (\kappa_s, \sigma_s)$	(κ_d, σ_d) and (κ_s, σ_s)

Table 4: Three different scenarios for which we will determine the NP parameters.

we are not making any assumptions regarding the origin of the NP. We will use Eqs. (82) and (83) to explore three different NP scenarios, which are summarised in Table 4.

Scenario I represents the most general case, and has the least assumptions. We utilise the UT apex determination in Section 2.3 for the SM predictions of the mixing parameters Δm_q and ϕ_q , together with the numerical values given in Section 3.1, to determine the NP parameters (κ_d, σ_d) and (κ_s, σ_s) independently from each other.

For the second and third scenario, we explore other options that require additional assumptions. In Scenario II we consider the case where NP contributions are equal in the B_d and the B_s systems, i.e. FUNP. Note that this is different from the well-known Minimal Flavour Violation scenario, which assumes no CP-violating NP phase at all, as was already noted in Ref. [1], where the same scenario was studied. Assuming the FUNP framework, it is possible to employ the UT apex determination that only relies on R_b and the mixing parameters described in Section 3.2, without requiring additional information on γ . In this way, possible NP in γ will not affect the results. However, assuming that NP affects the B_d and B_s systems equally is a strong assumption. A comparison of the FUNP scenario with the general scenario provides a test of the FUNP assumption and gives a measure of the impact that these assumptions have on the constraints on the parameter space of NP in $B_q^0-\bar{B}_q^0$ mixing.

The last scenario we will discuss is an interpolation between Scenario I and II. We will assume FUNP to determine the UT apex, using only information from R_b and the mixing parameters, but will relax this assumption when determining (κ_d, σ_d) and (κ_s, σ_s) . This scenario has less stringent assumptions on the form of the NP than for the full FUNP scenario. Comparing it with Scenario I and II allows us both to estimate the impact of the FUNP assumption on the fit to the NP parameters, and to explore the impact of the different UT apex determinations.

4.1 Scenario I: General New Physics

Scenario I is a general determination of the NP parameters in $B_q^0-\bar{B}_q^0$ mixing, given in Eqs. (82) and (83). We will use our results from Section 2 including information from R_b and γ , together with the SM expressions and values for the mixing parameters, summarized in Table 3, to determine the NP parameters (κ_q, σ_q) . The only assumption that enters this scenario is the absence of NP in γ and the semileptonic decays needed to determine

R_b . The results are shown in Fig. 6 and given as follows:

$$\text{Incl, } K\ell 3 \quad \kappa_d = 0.121^{+0.056}_{-0.055}, \quad \sigma_d = (261^{+37}_{-35})^\circ, \quad (84)$$

$$\kappa_s = 0.045^{+0.048}_{-0.033}, \quad \sigma_s = (312^{+37}_{-77})^\circ, \quad (85)$$

$$\text{Excl, } K\ell 3 \quad \kappa_d = 0.156^{+0.093}_{-0.084}, \quad \sigma_d = (347^{+21}_{-25})^\circ, \quad (86)$$

$$\kappa_s = 0.205^{+0.064}_{-0.059}, \quad \sigma_s = (347.6^{+8.5}_{-9.8})^\circ, \quad (87)$$

$$\text{Hybrid, } K\ell 3 \quad \kappa_d = 0.031^{+0.057}_{-0.031}, \quad \sigma_d = (104^{+256}_{-104})^\circ, \quad (88)$$

$$\kappa_s = 0.053^{+0.046}_{-0.034}, \quad \sigma_s = (309^{+34}_{-65})^\circ. \quad (89)$$

We observe in Fig. 6 that the individual constraints from ϕ_d in the inclusive scenario and Δm_s in the exclusive scenario are in tension with the SM, while all other constraints are compatible with $\kappa_q = 0$.

A comparison of the two-dimensional confidence regions between the three fit solutions based on different values of R_b is given in Fig. 7, and a comparison between the fit solutions for the B_d and B_s systems in Fig. 8. The correlation between κ_d and κ_s is also shown in Fig. 9. As illustrated in Fig. 9, all three R_b solutions are compatible with the assumption $\kappa_d = \kappa_s$, which is used in the FUNP scenario. However, the conclusions regarding the presence of NP are different for the three scenarios: The inclusive one is compatible with $\kappa_s = 0$, but suggests $\kappa_d \neq 0$; the exclusive fit result is compatible with $\kappa_d = 0$, but finds κ_s different from zero with a significance of 3.5 standard deviations; and the hybrid case is compatible with both $\kappa_d = 0$ and $\kappa_s = 0$ and hence finds no tension with the SM.

4.2 Scenario II: Flavour Universal New Physics

In the second scenario, we will assume FUNP, where the size and phase of the NP contributions, κ_q and σ_q , are equal for the B_d and B_s systems:

$$\kappa_d = \kappa_s \equiv \kappa, \quad \sigma_d = \sigma_s \equiv \sigma. \quad (90)$$

An important consequence is that the NP effects drop out in the ratio $\Delta m_d/\Delta m_s$. This means that the side R_t of the UT, defined in Eq. (66), will receive no contributions from NP at order λ^2 . We can use the results for the UT apex coming from information from R_b and R_t , as given in Eqs. (71)–(73), to determine the SM values of Δm_q and ϕ_q without additional information on γ . Comparing the SM predictions to their experimental values, we get constraints on κ and σ . This results in the following fit values for κ and σ :

$$\text{Incl, } K\ell 3 \quad \kappa = 0.057^{+0.040}_{-0.026}, \quad \sigma = (294^{+34}_{-53})^\circ, \quad (91)$$

$$\text{Excl, } K\ell 3 \quad \kappa = 0.203^{+0.062}_{-0.057}, \quad \sigma = (347.7^{+7.4}_{-8.3})^\circ, \quad (92)$$

$$\text{Hybrid, } K\ell 3 \quad \kappa = 0.043^{+0.049}_{-0.036}, \quad \sigma = (326^{+32}_{-90})^\circ. \quad (93)$$

These results are very similar to those arising from the fit for the B_s system from R_b and γ in Eqs. (84)–(89), implying that the B_s system dominates these fits. In Fig. 8, we can see that in the exclusive case, the results for FUNP almost completely overlap with those of the B_s system for Scenario I. In the inclusive and hybrid scenarios, the shape of the contours for the B_d and the B_s system are very different, indicating that FUNP might not be a correct assumption. However, the solutions still overlap within the error margin, and one can see that the FUNP scenario interpolates between the B_d and B_s systems, with the B_s system still dominating. In all cases, we cannot rule out FUNP, as it is still compatible with the results from the general scenario for both B_d and B_s .

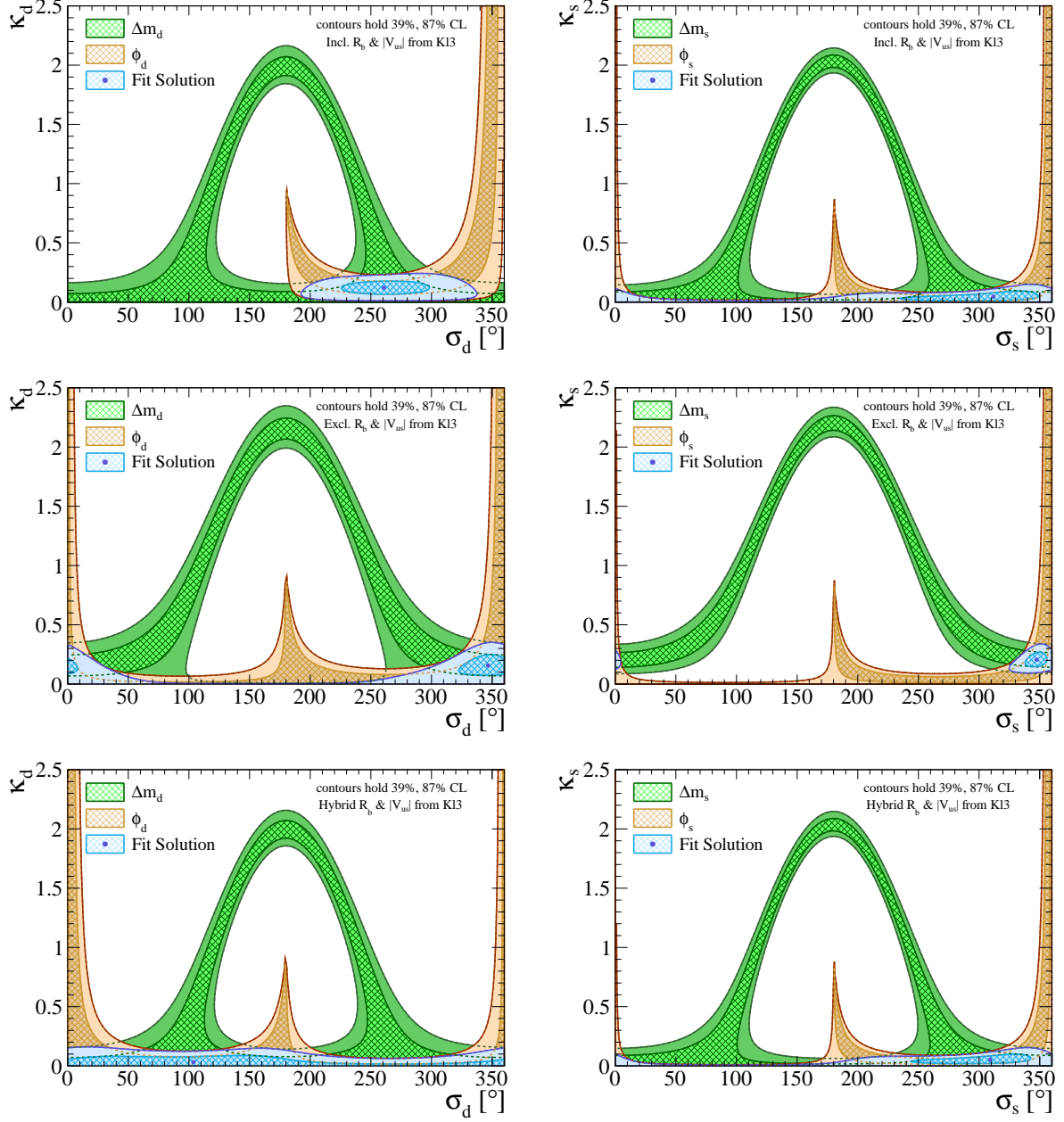


Figure 6: Two-dimensional confidence regions of the fit for κ_d and σ_d (left), and κ_s and σ_s (right), which parametrise NP contributions in $B_q^0 - \bar{B}_q^0$ mixing. For illustration, also the individual constraints from ϕ_q and Δm_q are shown. Top: Inclusive scenario. Middle: Exclusive scenario. Bottom: Hybrid scenario.

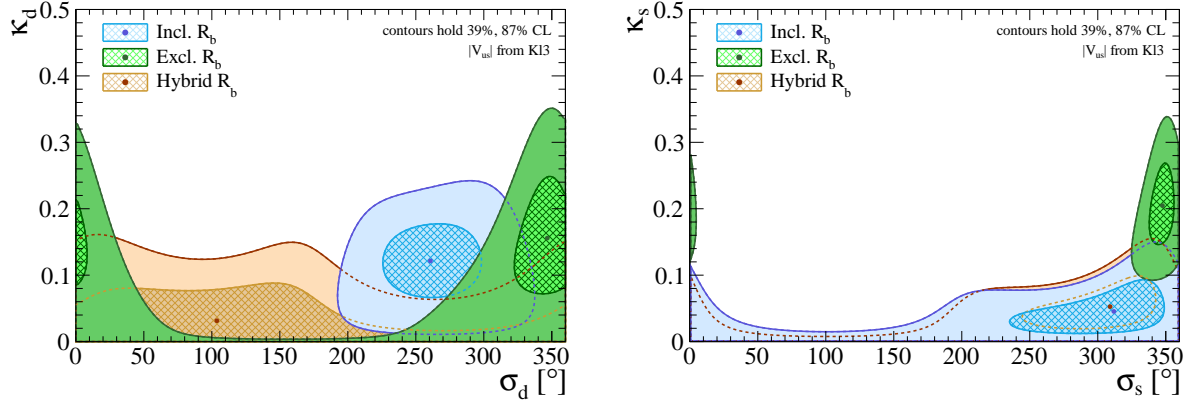


Figure 7: Comparison between the inclusive, exclusive and hybrid scenario of the two-dimensional confidence regions of the fits for κ_d and σ_d (left), and κ_s and σ_s (right), which parametrise NP contributions in $B_q^0-\bar{B}_q^0$ mixing.

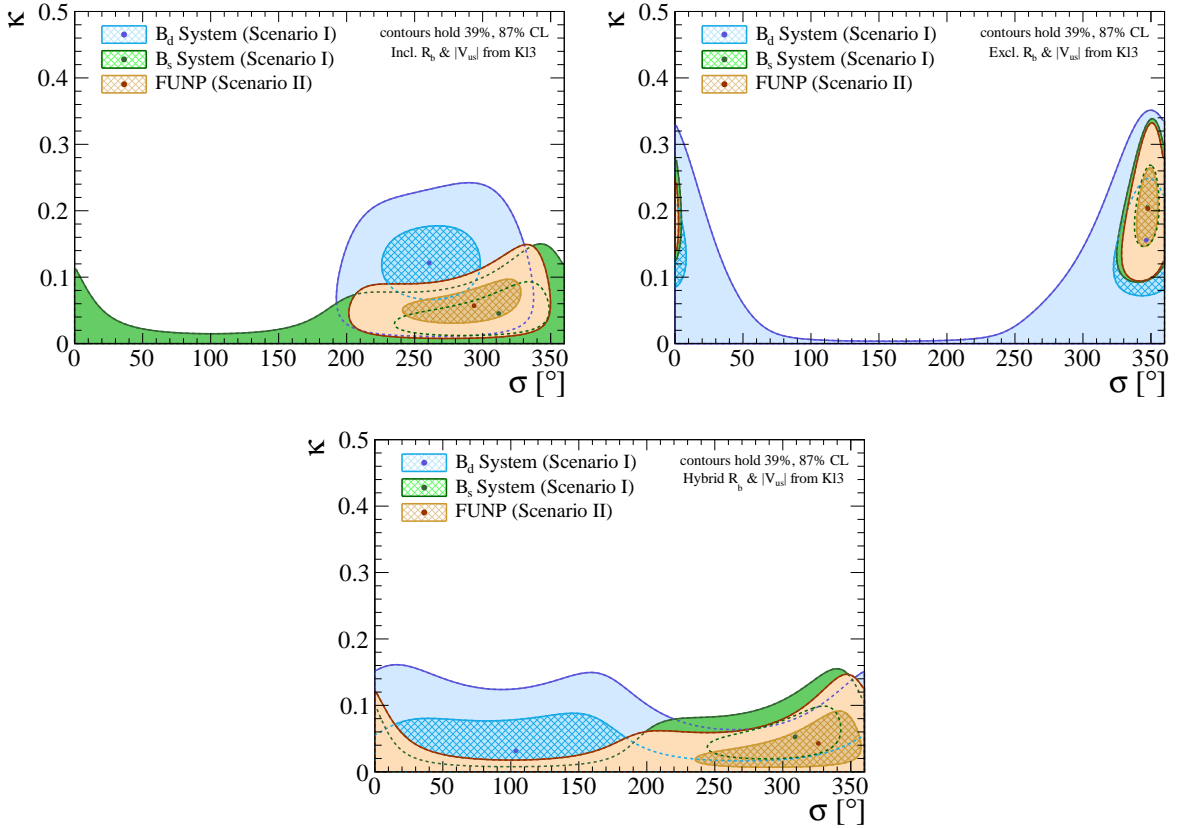


Figure 8: Comparison between the two-dimensional confidence regions of the Scenario I and Scenario II fits for κ_q and σ_q , which parametrise NP contributions in $B_q^0-\bar{B}_q^0$ mixing. Left: Inclusive scenario. Right: Exclusive scenario. Bottom: Hybrid scenario.

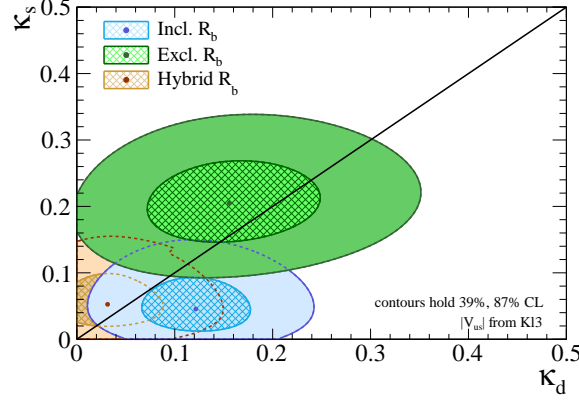


Figure 9: Comparison between the inclusive, exclusive and hybrid scenarios of the two-dimensional confidence regions of a combined fit for the NP parameters κ_d and κ_s describing NP contributions in $B_q^0\text{--}\bar{B}_q^0$ mixing. The black diagonal line represents the FUNP scenario, where $\kappa_d = \kappa_s$.

4.3 Scenario III: Going Beyond FUNP

Instead of assuming FUNP throughout the whole analysis to determine the NP parameters κ and σ , we can go beyond this scenario and relax the assumption of FUNP when fitting for the NP parameters. We will still assume FUNP to determine the UT apex, using only R_b and R_t without additional information from γ . However, we will determine (κ_d, σ_d) and (κ_s, σ_s) separately utilising the individual measurements of $\Delta m_d, \Delta m_s, \phi_d$ and ϕ_s . This results in the following picture:

$$\text{Incl, } K\ell 3 \quad \kappa_d = 0.130_{-0.051}^{+0.054}, \quad \sigma_d = (282_{-30}^{+31})^\circ, \quad (94)$$

$$\kappa_s = 0.045_{-0.033}^{+0.047}, \quad \sigma_s = (309_{-76}^{+38})^\circ, \quad (95)$$

$$\text{Excl, } K\ell 3 \quad \kappa_d = 0.208_{-0.078}^{+0.085}, \quad \sigma_d = (350_{-18}^{+10})^\circ, \quad (96)$$

$$\kappa_s = 0.203_{-0.059}^{+0.063}, \quad \sigma_s = (347.2_{-9.9}^{+8.6})^\circ, \quad (97)$$

$$\text{Hybrid, } K\ell 3 \quad \kappa_d = 0.050_{-0.050}^{+0.069}, \quad \sigma_d = (41_{-41}^{+319})^\circ, \quad (98)$$

$$\kappa_s = 0.052_{-0.032}^{+0.046}, \quad \sigma_s = (307_{-65}^{+34})^\circ. \quad (99)$$

The two-dimensional confidence regions are shown in Fig. 10. The solutions for the B_s system are identical to the NP fits based on R_b and γ in Scenario I. This can be explained as follows: Although the solution for the UT apex determined through R_b and R_t differs slightly from the solution obtained with R_b and γ , this difference only affects the value of $\bar{\rho}$. It therefore does not noticeably impact the SM prediction for ϕ_s , which only depends on $\bar{\eta}$. In addition, for both ϕ_s and Δm_s the dependence on the UT apex is suppressed by a factor λ^2 . Thus the SM predictions and experimental inputs for the NP fit in the B_s system are essentially identical for Scenario I and III. This is not the case for the B_d system. The NP searches in the B_d system are limited by the SM prediction for the UT apex, and thus sensitive to the difference between the R_b and γ scenario on the one hand, and the R_b and R_t scenario on the other. Nonetheless, as can be seen from the comparison in Fig. 10, the difference is small.

We can draw a similar conclusion as for the comparison between Scenario I and Scenario II. The solutions for the B_d and B_s systems are statistically compatible with

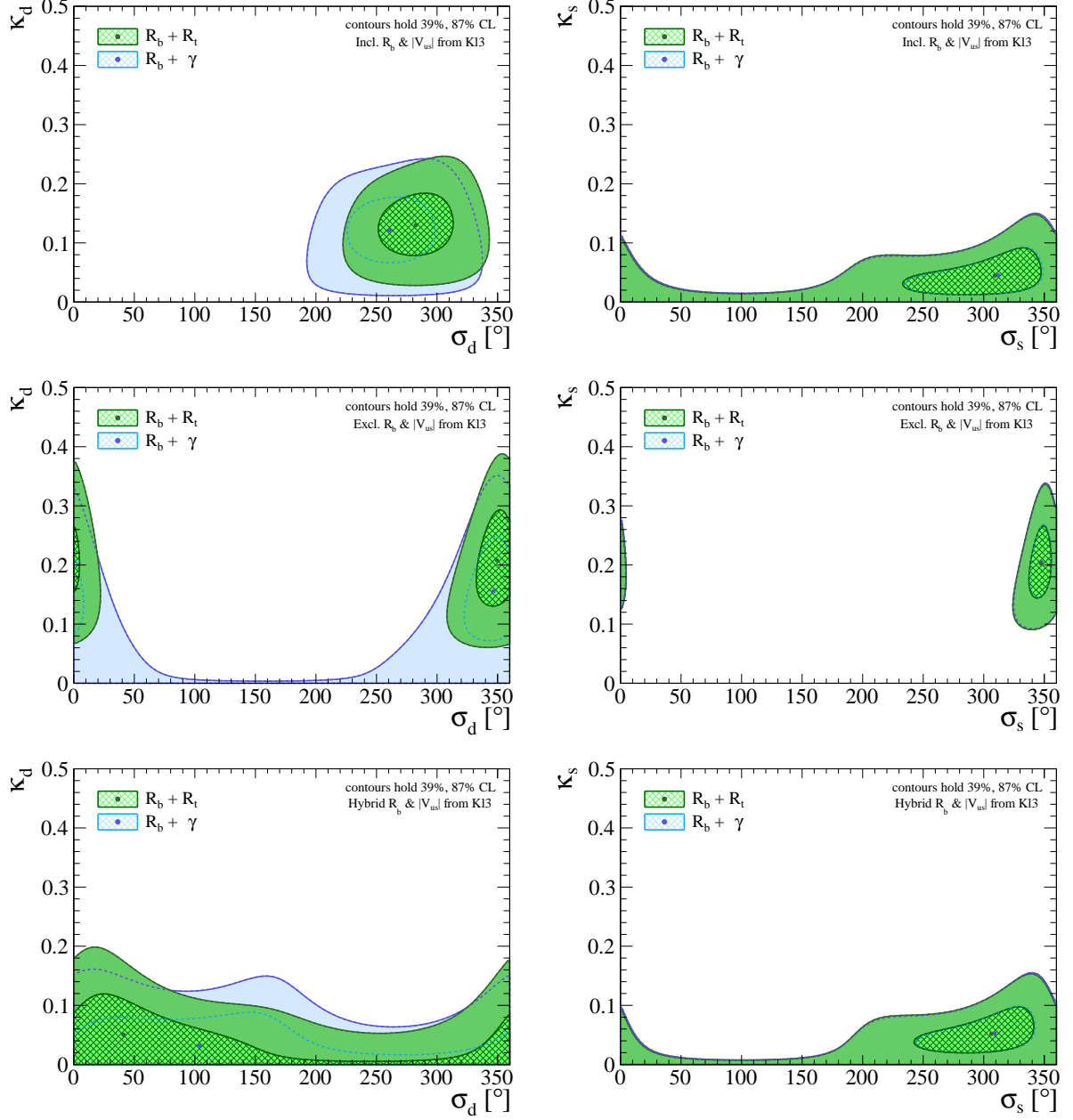


Figure 10: Comparison of the two-dimensional confidence regions of the Scenario I (labelled $R_b + \gamma$) and Scenario III (labelled $R_b + R_t$) fits for κ_d and σ_d (Left), and κ_s and σ_s (Right), which parametrise NP contributions in $B_q^0\text{--}\bar{B}_q^0$ mixing. Top: Inclusive scenario. Middle: Exclusive scenario. Bottom: Hybrid scenario.

each other, but do not look the same. This indicates that the data would favour a non-FUNP scenario, but we cannot exclude the FUNP scenario with the current precision.

Parameter	Value	Unit	Reference
\hat{B}_s	1.232 ± 0.053		[43, 61]
\hat{B}_s/\hat{B}_d	1.008 ± 0.025		[43, 61]
$2y_s \equiv \Delta\Gamma_s/\Gamma_s$	0.128 ± 0.007		[27]
$2y_d \equiv \Delta\Gamma_d/\Gamma_d$	0.001 ± 0.010		[27]
$\tau_{\mu\mu}^s$	2.07 ± 0.29	ps	[65]
τ_{B_s}	1.520 ± 0.005	ps	[27]
f_{B_s}	230.3 ± 1.3	MeV	[43]
$\tau_{B_s, H}$	1.624 ± 0.009	ps	[27]
η_Y	1.0113		[66]

Table 5: Input values for the SM computation of the $B_q^0 \rightarrow \mu^+\mu^-$ branching fractions. $\tau_{B_s, H}$ is the lifetime of the heavy B_s mass eigenstate and can be expressed in terms of τ_{B_s} and y_s as $\tau_{B_s}/(1 - y_s)$

5 Applications for the Rare Decays $B_q^0 \rightarrow \mu^+\mu^-$

The NP searches in the rare decays $B_q^0 \rightarrow \mu^+\mu^-$ are also affected by our choices for the CKM matrix elements. The SM predictions for the branching fractions are, using unitarity of the CKM matrix, proportional to the square of $|V_{cb}|$, and thus differ between the inclusive and exclusive determinations. Refs. [21–23] suggested to take the ratio with Δm_q in order to eliminate this dependence on $|V_{cb}|$. However, as we have seen above, Δm_q may be affected by NP effects. Using our analyses we are able to take these effects into account, and show the resulting constraints on NP in $B_s^0 \rightarrow \mu^+\mu^-$. In addition, we will also explore the option of using the ratio of $B_d^0 \rightarrow \mu^+\mu^-$ and $B_s^0 \rightarrow \mu^+\mu^-$ branching fractions to determine the UT side R_t , providing us with a second opportunity to determine the UT apex without relying on the angle γ .

5.1 $B_s^0 \rightarrow \mu^+\mu^-$ in the Standard Model

At lowest order in the SM, the “theoretical” branching fraction of the decay $B_s^0 \rightarrow \mu^+\mu^-$ is given as [67]

$$\mathcal{B}(B_s \rightarrow \mu^+\mu^-) = \frac{\tau_{B_s} G_F^4 m_W^4 \sin^4 \theta_W}{8\pi^5} |C_{10}^{\text{SM}}|^2 |V_{ts} V_{tb}^*|^2 f_{B_s}^2 m_{B_s} m_\mu^2 \sqrt{1 - \frac{4m_\mu^2}{m_{B_s}^2}}, \quad (100)$$

where θ_W is the weak mixing angle, and τ_{B_s} is the B_s -meson lifetime. The theoretical branching fraction is defined at decay time $t = 0$ and thus does not include effects coming from $B_s^0 - \bar{B}_s^0$ mixing. This is not the case for the experimentally measured time-integrated branching fraction, which is related to the theoretical branching fraction as follows [68]:

$$\bar{\mathcal{B}}(B_s \rightarrow \mu^+\mu^-) = \frac{1 + \mathcal{A}_{\Delta\Gamma}^{\mu\mu} y_s}{1 - y_s^2} \mathcal{B}(B_s \rightarrow \mu^+\mu^-), \quad (101)$$

where $\mathcal{A}_{\Delta\Gamma}^{\mu\mu} = 1$ in the SM. The parameter y_s is defined as

$$y_s \equiv \frac{\tau_{B_s}}{2} \Delta\Gamma_s, \quad (102)$$

where $\Delta\Gamma_s$ is the decay width difference between the B_s mass eigenstates. It is now clear that $B_q^0\text{--}\bar{B}_q^0$ mixing effects will affect the time-integrated branching fraction. The Wilson coefficient C_{10} can be expressed as

$$C_{10}^{\text{SM}} = \frac{\eta_Y Y_0(x_t)}{\sin^2 \theta_W}, \quad (103)$$

where η_Y is a QCD correction factor [66], and Y_0 is the Inami–Lim function [53]

$$Y_0(x) = \frac{x}{8} \left[\frac{4-x}{1-x} + \frac{3x}{(1-x)^2} \ln x \right]. \quad (104)$$

It is interesting to note that in this specific parametrisation the dependence on $\sin^2 \theta_W$ drops out from the theoretical prediction (100).

The SM branching fraction depends both on the value of $|V_{cb}|$ and on the solution of the UT apex through the relation (55) for the CKM matrix elements $|V_{ts}V_{tb}^*|$, although the latter dependence enters only through higher order corrections. This results in different predictions for the three scenarios considered in this paper:

$$\text{Incl, } K\ell 3 \quad \bar{\mathcal{B}}(B_s \rightarrow \mu^+ \mu^-) = (3.81 \pm 0.11) \times 10^{-9}, \quad (105)$$

$$\text{Excl, } K\ell 3 \quad \bar{\mathcal{B}}(B_s \rightarrow \mu^+ \mu^-) = (3.27 \pm 0.10) \times 10^{-9}, \quad (106)$$

$$\text{Hybrid, } K\ell 3 \quad \bar{\mathcal{B}}(B_s \rightarrow \mu^+ \mu^-) = (3.80 \pm 0.10) \times 10^{-9}. \quad (107)$$

In comparison with the latest prediction [69]

$$\bar{\mathcal{B}}(B_s \rightarrow \mu^+ \mu^-)|_{\text{SM}} = (3.66 \pm 0.14) \times 10^{-9} \quad (108)$$

found in the literature, our uncertainties are slightly smaller. This is primarily because the experimental measurements for the CKM matrix elements and top quark mass have improved compared to what was used in Ref. [69]. It is important to point out that the result (108) includes NLO electroweak and QCD corrections, while our predictions in Eqs. (105)–(107) are based on the LO expression only. We have not included NLO corrections since our goal is to illustrate the dependence of the numerical prediction on the choice for the CKM matrix elements and UT apex. This introduces a spread, as illustrated in Fig. 11, that is still much larger and thus more important than the NLO corrections.

On the experimental side, the $B_s^0 \rightarrow \mu^+ \mu^-$ branching fraction has been measured by the LHCb [65], ATLAS [70] and CMS [71, 72] collaborations. Their results are compared to the SM predictions in Fig. 11. In the context of the discussion on the $b \rightarrow s \ell \ell$ anomalies, multiple groups [73–75] have performed averages for these results, which are also shown in Fig. 11. The recent update [72] from CMS is not yet included in these averages. For the analysis below, we choose the result from Ref. [75]:

$$\bar{\mathcal{B}}(B_s \rightarrow \mu^+ \mu^-) = (2.85_{-0.31}^{+0.34}) \times 10^{-9}. \quad (109)$$

This average differs from the SM prediction (106) by one standard deviation, and from the SM predictions (105) and (107) by 2.4 standard deviations. Individual measurements of the $B_d^0 \rightarrow \mu^+ \mu^-$ branching fraction are not yet significantly different from zero. The LHCb [65], ATLAS [70] and CMS [71] results therefore only provide an upper limit, with the most stringent upper bound given by [65]

$$\bar{\mathcal{B}}(B_d \rightarrow \mu^+ \mu^-) < 0.26 \times 10^{-9}. \quad (110)$$

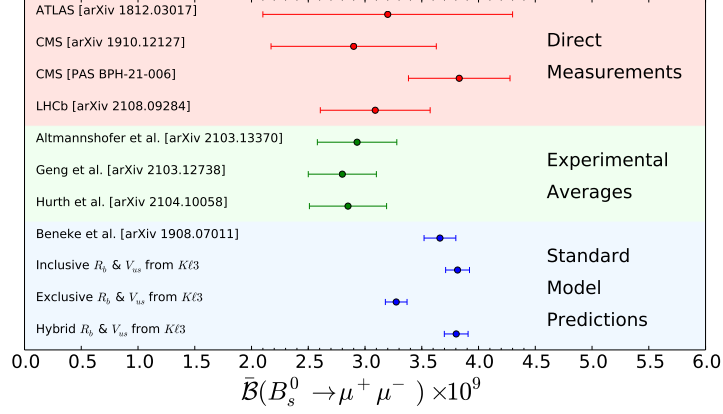


Figure 11: Comparison of the experimental measurements, averages and SM predictions for the time-integrated branching fraction $\bar{\mathcal{B}}(B_s^0 \rightarrow \mu^+ \mu^-)$

Nonetheless, based on the combined analysis with $B_s^0 \rightarrow \mu^+ \mu^-$, Ref. [74] does give the average

$$\bar{\mathcal{B}}(B_d \rightarrow \mu^+ \mu^-) = (0.56 \pm 0.70) \times 10^{-10}. \quad (111)$$

This result is still compatible with zero within one standard deviation.

5.2 Determining NP in $\bar{\mathcal{B}}(B_s \rightarrow \mu^+ \mu^-)$

NP can modify the $B_s^0 \rightarrow \mu^+ \mu^-$ branching fraction through pseudo-scalar (P) or scalar (S) contributions, or through B_s^0 - \bar{B}_s^0 mixing. The measured $B_s^0 \rightarrow \mu^+ \mu^-$ branching fraction is given by

$$\bar{\mathcal{B}}(B_s \rightarrow \mu^+ \mu^-) = \bar{\mathcal{B}}(B_s \rightarrow \mu^+ \mu^-)^{\text{SM}} \times \frac{1 + \mathcal{A}_{\Delta\Gamma_s}^{\mu\mu} y_s}{1 + y_s} (|P_{\mu\mu}^s|^2 + |S_{\mu\mu}^s|^2), \quad (112)$$

where $\mathcal{A}_{\Delta\Gamma_s}^{\mu\mu}$ depends on $P_{\mu\mu}^s \equiv |P_{\mu\mu}^s| e^{i\varphi_P}$, $S_{\mu\mu}^s \equiv |S_{\mu\mu}^s| e^{i\varphi_S}$ and ϕ_s^{NP} as

$$\mathcal{A}_{\Delta\Gamma}^{\mu\mu} = \frac{|P_{\mu\mu}^s|^2 \cos(2\varphi_P - \phi_s^{\text{NP}}) - |S_{\mu\mu}^s|^2 \cos(2\varphi_S - \phi_s^{\text{NP}})}{|P_{\mu\mu}^s|^2 + |S_{\mu\mu}^s|^2}. \quad (113)$$

In the SM, we have

$$P_{\mu\mu}^{s,\text{SM}} = 1, \quad S_{\mu\mu}^{s,\text{SM}} = 0. \quad (114)$$

Comparing the experimental average (109) with the SM predictions (105)-(107), we can constrain the parameters $|P_{\mu\mu}^s|$ and $|S_{\mu\mu}^s|$, as proposed in Ref. [68]. For the scenario where the NP phases for the pseudo-scalar and scalar contributions are zero, i.e. $\varphi_P = \varphi_S = 0$, the results are shown in Fig. 12.

The dependence of the NP searches with $\bar{\mathcal{B}}(B_s \rightarrow \mu^+ \mu^-)$ on the CKM matrix element $|V_{cb}|$ and the UT apex, which is clearly visible when comparing the blue contours in Fig. 12, can be minimised by constructing the ratio with the B_s mass difference Δm_s [21–23]:

$$\mathcal{R}_{s\mu} \equiv \left| \frac{\bar{\mathcal{B}}(B_s \rightarrow \mu^+ \mu^-)}{\Delta m_s} \right|. \quad (115)$$

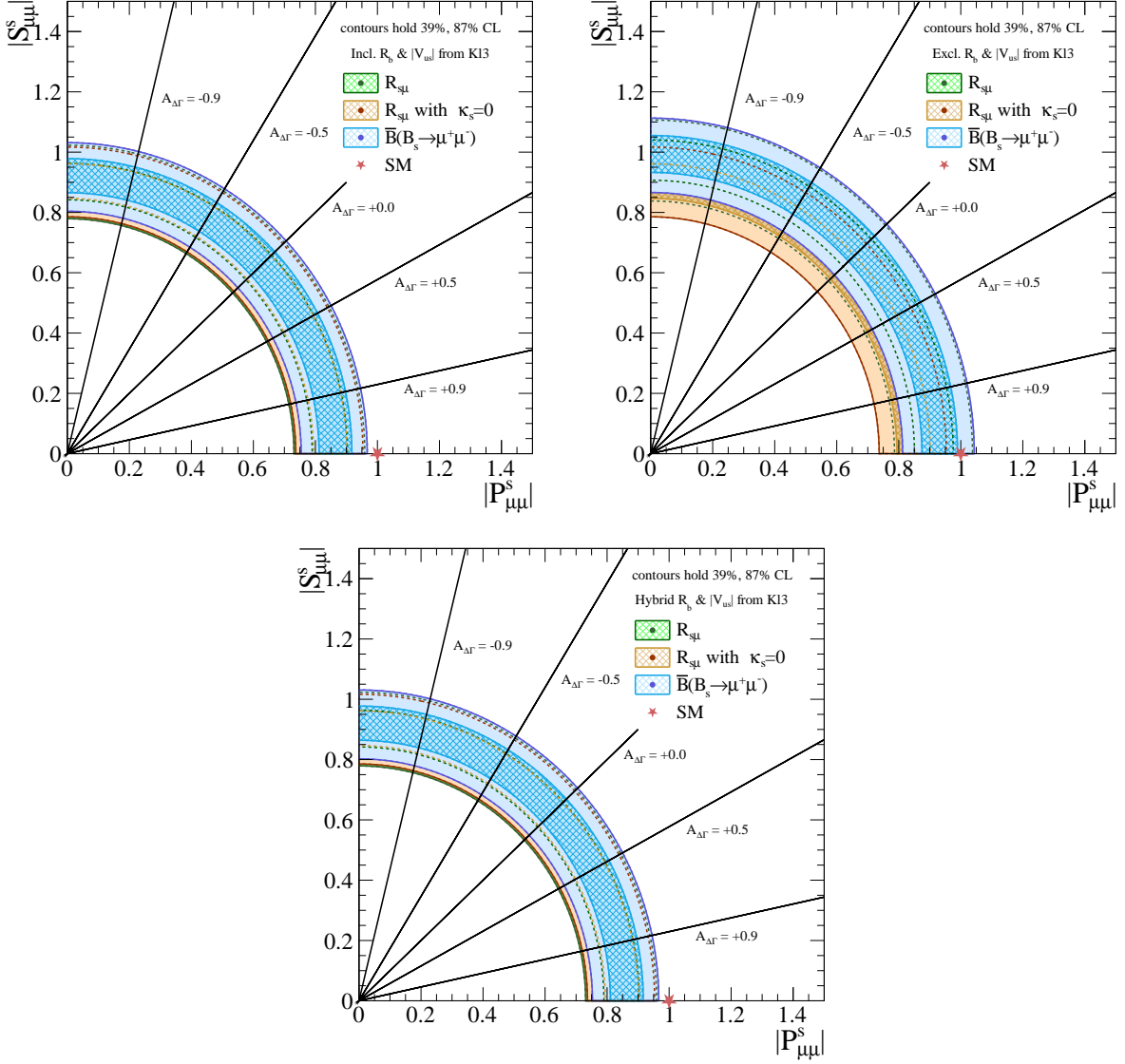


Figure 12: Two-dimensional confidence regions for the constraints from $\mathcal{B}(B_s \rightarrow \mu^+\mu^-)$ and $R_{s\mu}$ on $|P_{\mu\mu}^s|$ and $|S_{\mu\mu}^s|$, assuming $\varphi_P = \varphi_S = 0$. Left: Inclusive scenario. Right: Exclusive scenario. Bottom: Hybrid scenario.

At lowest order, the SM contribution is given by

$$\mathcal{R}_{s\mu}^{\text{SM}} = \frac{\tau_{B_s}}{1 - y_s} \frac{3G_F^2 m_W^2 \sin^4 \theta_W}{4\pi^3} \frac{|C_{10}^{\text{SM}}|^2}{S_0(x_t) \eta_{2B} \hat{B}_{B_s}} m_\mu^2 \sqrt{1 - 4 \frac{m_\mu^2}{m_{B_s}^2}}, \quad (116)$$

resulting in the prediction

$$\mathcal{R}_{s\mu}^{\text{SM}} = (2.22 \pm 0.10) \times 10^{-10} \text{ ps}. \quad (117)$$

Including NLO corrections Ref. [22] finds a similar result

$$\mathcal{R}_{s\mu}^{\text{SM}} = (2.042^{+0.083}_{-0.058}) \times 10^{-10} \text{ ps}, \quad (118)$$

which differs from ours due to the choice for the bag parameter \hat{B}_{B_s} . Also here, the choices made for the input parameters still have a bigger impact than the NLO corrections.

Including NP effects in both $\bar{\mathcal{B}}(B_s \rightarrow \mu^+\mu^-)$ and Δm_s , the expression for the ratio $\mathcal{R}_{s\mu}$ is generalised as follows:

$$\mathcal{R}_{s\mu} = \mathcal{R}_{s\mu}^{\text{SM}} \times \frac{1 + \mathcal{A}_{\Delta\Gamma_s}^{\mu\mu} y_s}{1 + y_s} \frac{|P_{\mu\mu}^s|^2 + |S_{\mu\mu}^s|^2}{\sqrt{1 + 2\kappa_s \cos \sigma_s + \kappa_s^2}}. \quad (119)$$

It is important to stress that although the leading dependence on the CKM matrix elements drops out in Eq. (116) because we take the ratio with respect to Δm_s , the ratio in Eq. (119) introduces a dependence on the CKM matrix elements through the NP parameters (κ_s, σ_s) . Hence, when taking into account NP effects in B_q^0 - \bar{B}_q^0 mixing, one should stay careful with the choice of the input of the CKM matrix elements.

Combining the experimental results in Eqs. (109) and (61), we get

$$\mathcal{R}_{s\mu} = (1.60 \pm 0.19) \times 10^{-10}. \quad (120)$$

Comparing this with the SM value, we can again obtain contours in the $|P_{\mu\mu}^s|$ - $|S_{\mu\mu}^s|$ plane. These are also shown in Fig. 12 for the scenario where the NP phases for the pseudo-scalar and scalar contributions are zero.

5.3 Using $\bar{\mathcal{B}}(B_q \rightarrow \mu^+\mu^-)$ to Extract R_t

In Section 3.2, we introduced an alternative determination of the SM UT apex based on the sides R_b and R_t , avoiding the use of the angle γ . This second UT fit scenario becomes interesting when searching for potential NP contributions in the measurements of γ . However, its main limitation is the calculation of the side R_t based on the ratio of CKM matrix elements $|V_{td}/V_{ts}|$, which is susceptible to NP contributions as well. In Eq. (67), this ratio was determined using the B_q^0 - \bar{B}_q^0 mixing parameters. Here we would like to explore the determination of the ratio $|V_{td}/V_{ts}|$ using the rare decays $B_q^0 \rightarrow \mu^+\mu^-$. In the SM and FUNP scenario, the result would be consistent with the strategy based on Δm_s and Δm_d , which can be tested experimentally.

Based on the SM expressions in Eqs. (100) and (101), the ratio of branching fractions between $B_d^0 \rightarrow \mu^+\mu^-$ and $B_s^0 \rightarrow \mu^+\mu^-$ is given by

$$\left. \frac{\bar{\mathcal{B}}(B_d \rightarrow \mu^+\mu^-)}{\bar{\mathcal{B}}(B_s \rightarrow \mu^+\mu^-)} \right|_{\text{SM}} = \lambda^2 R_t^2 \left[1 + \frac{\lambda^2}{2} (1 - 2\bar{\rho}) \right]^2 \frac{\sqrt{m_{B_d}^2 - 4m_\mu^2} f_{B_d}^2 \frac{1 - y_s}{1 - y_d}}{\sqrt{m_{B_s}^2 - 4m_\mu^2} f_{B_s}^2}, \quad (121)$$

where we used Eq. (66) to rewrite the ratio $|V_{td}/V_{ts}|$ in terms of the UT side R_t . Combining this with the SM values for R_t given in Eqs. (71)–(73), which are calculated using R_b and γ , and using $f_{B_s}/f_{B_d} = 1.209 \pm 0.005$ [43], we get the predictions:

$$\text{Incl, } K\ell 3 \quad \left. \frac{\bar{\mathcal{B}}(B_d \rightarrow \mu^+\mu^-)}{\bar{\mathcal{B}}(B_s \rightarrow \mu^+\mu^-)} \right|_{\text{SM}} = 0.0282 \pm 0.0019, \quad (122)$$

$$\text{Excl, } K\ell 3 \quad \left. \frac{\bar{\mathcal{B}}(B_d \rightarrow \mu^+\mu^-)}{\bar{\mathcal{B}}(B_s \rightarrow \mu^+\mu^-)} \right|_{\text{SM}} = 0.0281 \pm 0.0018, \quad (123)$$

$$\text{Hybrid, } K\ell 3 \quad \left. \frac{\bar{\mathcal{B}}(B_d \rightarrow \mu^+\mu^-)}{\bar{\mathcal{B}}(B_s \rightarrow \mu^+\mu^-)} \right|_{\text{SM}} = 0.0281 \pm 0.0017. \quad (124)$$

The difference between the three R_b scenarios is almost negligible given the current precision. This suggests a high-precision measurement of the $B_q^0 \rightarrow \mu^+\mu^-$ branching fractions will be necessary to constrain R_t through this method.

In contrast, the current experimental result for the ratio of branching fractions, based on Ref. [74] that gives the average for $\bar{\mathcal{B}}(B_d \rightarrow \mu^+\mu^-)$ in Eq. (111), is

$$\frac{\bar{\mathcal{B}}(B_d \rightarrow \mu^+\mu^-)}{\bar{\mathcal{B}}(B_s \rightarrow \mu^+\mu^-)} = 0.019 \pm 0.024, \quad (125)$$

and has an uncertainty of 125%. This corresponds to a value for the UT side R_t of

$$R_t = 0.77 \pm 0.48. \quad (126)$$

In comparison with the determinations in Eqs. (74)–(79) the uncertainty is a factor 20 to 40 larger. However, with the third data taking period of the LHC just started, more precise measurements of the $B_q^0 \rightarrow \mu^+\mu^-$ branching fractions can be expected in the near future, thereby making this an interesting option to explore, and useful addition to the study of NP effects in $B_q^0\text{--}\bar{B}_q^0$ mixing.

6 What Will the Future Bring?

6.1 Improved Precision on the NP Parameters κ_q and σ_q

The NP searches in $B_q^0\text{--}\bar{B}_q^0$ mixing are limited by the SM predictions for ϕ_d , Δm_d and Δm_s . Only the SM value for ϕ_s is still more precisely known than its experimental measurement. The value of ϕ_d^{SM} is limited by our knowledge of the UT apex, and in particular R_b , while the largest uncertainty in the calculations of Δm_d^{SM} and Δm_s^{SM} are due to the non-perturbative parameters. Improving these calculations has turned out to be difficult, and the associated time-scale unpredictable. We therefore refrain from making specific estimates for the future. Instead we will only illustrate the impact that improvements on the UT apex, lattice calculations and the CKM matrix element $|V_{cb}|$ have on the NP parameters κ_q and σ_q , and explore their relative importance. Table 6 numerically compares the current precision on κ_q and σ_q with what is achievable assuming a hypothetical reduction of the uncertainty on each of these three inputs by 50%. For the two inputs that have the largest impact, the two-dimensional confidence level contours are compared in Fig. 13.

For the B_s -meson system, the precision on κ_s and σ_s is limited by the uncertainty on the lattice calculations. Improvements to these calculations will reduce the allowed confidence region the most, and are therefore eagerly anticipated. In contrast, the impact from improvements in our knowledge of the UT apex is essentially negligible. This is in particular the case for ϕ_s . In Ref. [76], discussing the prospects for LHCb Upgrade II, an experimental precision on the measurement of ϕ_s^{eff} from $B_s^0 \rightarrow J/\psi\phi$ of 4 mrad was forecasted. This is still a factor 2 bigger than the current precision on ϕ_s^{SM} , given in Eqs. (46)–(48). The search for NP in ϕ_s will thus remain limited by the experimental data, irrespective of our knowledge on the UT apex. This conclusion was already noted in Ref. [6], and can be easily understood: Both ϕ_s^{SM} and Δm_s^{SM} only depend on $\bar{\rho}$ and $\bar{\eta}$ at next-to-leading order, and their contributions are suppressed by a factor λ^2 compared to the leading order terms, while the lattice parameters appear quadratically in the leading

order expression of Δm_s^{SM} . Also $|V_{cb}|$ appears quadratically in Δm_s^{SM} , but the impact of an improved measurement remains small as long as the lattice results dominate the error budget.

The future prospects for finding NP in the B_s -meson system are highly dependent on the assumptions made. From the considered scenarios shown in Fig. 13, the exclusive scenario assuming a 50% improvement from lattice appears most exciting. If this were to be realised, we could claim NP in $B_s^0-\bar{B}_s^0$ mixing with a significance of more than 5 standard deviations. In the other scenarios, the situation will be more challenging.

For the B_d -meson system, the situation is very different. Here, improvements in the determination of the UT apex and the reduction of the uncertainties from lattice calculations have an equally big impact on the allowed confidence regions for κ_d and σ_d . In particular, the limitation due to the UT apex is surprising, as was also pointed out in Ref. [36] in the context of NP searches in ϕ_d . The uncertainties on the SM predictions for ϕ_d in Eqs. (42)–(44) are about 40% larger than the uncertainty on the experimental measurement in Eq. (10). This situation will not significantly change in the near future, as we can illustrate using the forecasts for the LHCb Upgrade II [76]. LHCb expects to reduce the uncertainty on R_b to 1% and on γ to 0.35° by the end of the HL-LHC programme. This corresponds to a precision on ϕ_d^{SM} of 0.48° . By contrast, LHCb expects to be able to measure the mixing-induced CP asymmetry of the decay $B_d^0 \rightarrow J/\psi K_S^0$ with an uncertainty of only 0.003. This corresponds to a precision on ϕ_d^{eff} of 0.24° , and can be translated to a measurement of ϕ_d after taking into account the contributions from higher-order penguin topologies. In Ref. [36], we argued that it is possible to control these penguin corrections with similar experimental precision, thus resulting in an estimated precision on ϕ_d of 0.34° . Thus at the end of the HL-LHC programme, the uncertainty on the SM prediction will still be 40% larger than the experimental measurement. Measurements from the Belle II experiment will help to reduce this difference, but cannot completely bridge the gap in precision. This makes it all the more important to critically analyse the UT fit and carefully select its inputs. The determination of the SM values of $\bar{\rho}$ and $\bar{\eta}$ should remain a high priority as it impacts the vast majority of NP searches, ranging from $B_q^0-\bar{B}_q^0$ mixing to rare decays like $B_q^0 \rightarrow \mu^+\mu^-$.

The future prospects for finding NP in the B_d -meson system are again highly dependent on the assumptions made. From the considered scenarios shown in Fig. 13, the inclusive scenario assuming a 50% improvement on the UT apex stands out. Here, we could find hints for NP in $B_d^0-\bar{B}_d^0$ mixing with a significance of more than 3 standard deviations. This is less promising than the B_s -meson system. The difference is mainly due to the smaller value we find for κ_d in the current data.

As a final remark, note that improvements on the non-perturbative parameters can also be achieved by combining the lattice calculations with LQSR results. However, dedicated averages like those provided by FLAG [43] for the lattice calculations are still missing. Nonetheless, such averages, if available, can have a significant impact on the study of B -meson decays, both on the NP searches in $B_q^0-\bar{B}_q^0$ mixing, and in the determination of $|V_{ub}|$ and $|V_{cb}|$, and thus the UT apex.

6.2 NP in γ

As discussed in Section 2.1, the two determinations of γ , based on the analysis of $B \rightarrow DK$ decays and based on the isospin analysis of the $B \rightarrow \pi\pi$, $\rho\pi$, $\rho\rho$ decays, are in good

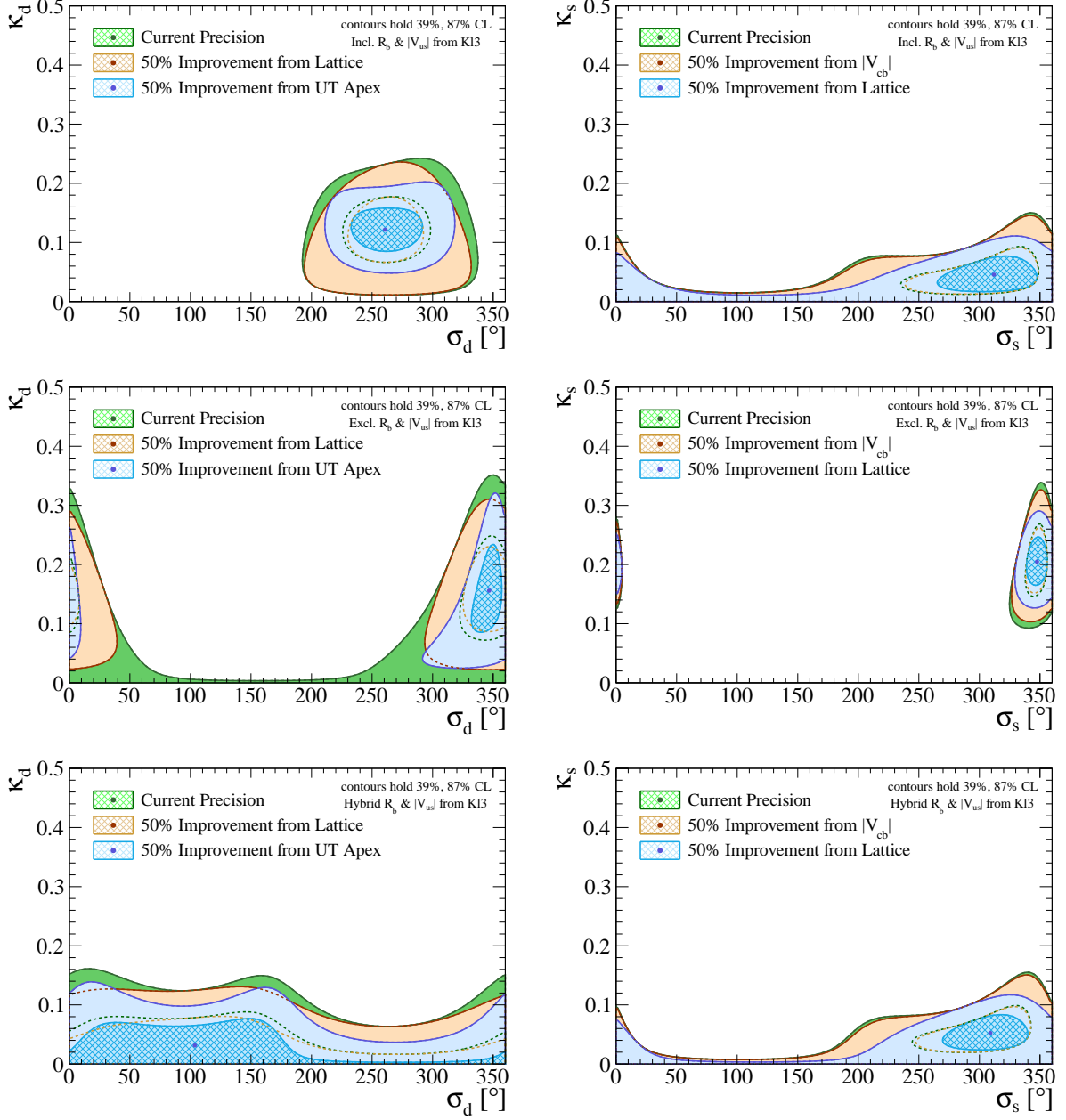


Figure 13: Comparison of the two-dimensional confidence regions for the NP parameters κ_d and σ_d (Left), and κ_s and σ_s (Right) assuming a hypothetical reduction of 50% in the uncertainty on the CKM matrix element $|V_{cb}|$, the lattice calculations, or the UT apex. Top: Inclusive scenario. Middle: Exclusive scenario. Bottom: Hybrid scenario.

Fit	Scenario	κ_q	$\sigma(\kappa_q)$	σ_q	$\sigma(\sigma_q)$
B_d I3	Current	0.121	$-0.055/+0.056$	261°	$-35^\circ/+37^\circ$
	50% improvement $ V_{cb} $	0.121	$-0.055/+0.056$	261°	$-35^\circ/+37^\circ$
	50% improvement lattice	0.121	$-0.055/+0.056$	261°	$-31^\circ/+31^\circ$
	50% improvement UT apex	0.121	$-0.036/+0.037$	261°	$-28^\circ/+31^\circ$
B_d E3	Current	0.156	$-0.084/+0.093$	347°	$-25^\circ/+21^\circ$
	50% improvement $ V_{cb} $	0.156	$-0.081/+0.089$	347°	$-24^\circ/+21^\circ$
	50% improvement lattice	0.156	$-0.069/+0.074$	347°	$-22^\circ/+21^\circ$
	50% improvement UT apex	0.156	$-0.071/+0.078$	347°	$-15^\circ/+10^\circ$
B_d H3	Current	0.031	$-0.031/+0.057$	104°	$-104^\circ/+256^\circ$
	50% improvement $ V_{cb} $	0.031	$-0.031/+0.056$	104°	$-104^\circ/+256^\circ$
	50% improvement lattice	0.031	$-0.031/+0.050$	104°	$-104^\circ/+256^\circ$
	50% improvement UT apex	0.031	$-0.031/+0.046$	104°	$-104^\circ/+256^\circ$
B_s I3	Current	0.045	$-0.033/+0.048$	312°	$-77^\circ/+37^\circ$
	50% improvement $ V_{cb} $	0.045	$-0.032/+0.046$	312°	$-73^\circ/+37^\circ$
	50% improvement lattice	0.045	$-0.028/+0.032$	312°	$-47^\circ/+36^\circ$
	50% improvement UT apex	0.045	$-0.033/+0.048$	312°	$-77^\circ/+37^\circ$
B_s E3	Current	0.205	$-0.059/+0.064$	347.6°	$-9.8^\circ/+8.5^\circ$
	50% improvement $ V_{cb} $	0.205	$-0.053/+0.058$	347.6°	$-9.4^\circ/+8.5^\circ$
	50% improvement lattice	0.205	$-0.040/+0.042$	347.6°	$-8.8^\circ/+8.5^\circ$
	50% improvement UT apex	0.205	$-0.059/+0.064$	347.6°	$-9.7^\circ/+8.5^\circ$
B_s H3	Current	0.053	$-0.034/+0.046$	309°	$-65^\circ/+34^\circ$
	50% improvement $ V_{cb} $	0.053	$-0.033/+0.044$	309°	$-61^\circ/+33^\circ$
	50% improvement lattice	0.053	$-0.029/+0.030$	309°	$-39^\circ/+31^\circ$
	50% improvement UT apex	0.053	$-0.034/+0.046$	309°	$-64^\circ/+34^\circ$

Table 6: Numerical comparison of the NP parameters κ_q and σ_q assuming a hypothetical reduction of 50% in the uncertainty on the CKM matrix element $|V_{cb}|$, the lattice calculations, or the UT apex. The fit results are given separately for the inclusive (I3), exclusive (E3) and hybrid (H3) R_b scenario with $|V_{us}|$ determined with the $K\ell 3$ approach.

agreement with each another. Given the very different origins of these measurements, this is a non-trivial result. In the future, improved precision on the input measurements to these analyses could result in discrepancies between the two γ determinations. Averaging over both results, as we have done in Section 2.1, would then no longer be justified, and the SM determination of the UT apex would have to be revisited. As it is a priori unclear which of the two measurements, if not both, is affected by NP contributions, independent information from additional observables will then be necessary to resolve the situation. At the same time, this will also provide exciting new opportunities to search for NP, both in γ itself and in $B_q^0\text{--}\bar{B}_q^0$ mixing, which is strongly correlated with the coordinates of the UT apex.

In Sections 3.2 and 5.3, we have explored alternative scenarios that do not rely on the measurements of γ . However, all these scenarios have a common bottleneck: the SM determination of R_t . Both the determination based on the measurements of Δm_d and Δm_s , and the determination based on the branching fractions of the rare decays $B_q^0 \rightarrow \mu^+ \mu^-$ require us to make additional assumptions about FUNP, such that the ratios

between the B_d and B_s observables remains SM-like. Although this may be sufficient to find evidence of NP, it does not allow for a general model-independent approach and exploring multiple strategies simultaneously may be necessary to understand the origin of the NP contributions.

6.3 Opportunities for $\bar{\mathcal{B}}(B_q \rightarrow \mu^+ \mu^-)$

The ratio of branching fractions between $B_d^0 \rightarrow \mu^+ \mu^-$ and $B_s^0 \rightarrow \mu^+ \mu^-$ provides an alternative opportunity to determine the UT side R_t . However, as the precision on R_t^2 scales directly with the precision on the ratio of branching fractions, the current experimental uncertainties are still too large to already explore this option in detail. But we can illustrate the potential for the LHC upgrade programme. The LHCb collaboration expects to be able to reduce the uncertainty on the ratio of branching fractions to 34% by 2025 and to 10% by the end of the HL-LHC era [76]. Assuming the SM value from Eqs. (77)–(79), this results in the prospects

$$R_t = 0.93 \pm 0.16 \text{ (2025)}, \quad R_t = 0.931 \pm 0.047 \text{ (Upgrade II)}, \quad (127)$$

where the uncertainties are still fully dominated by the branching fraction measurements. All other uncertainties combined only contribute at the 1% level and can thus safely be ignored. In comparison with the determinations in Eqs. (74)–(79), the LHCb Upgrade II prospects are still a factor 2 to 4 larger, as illustrated in Fig. 14. We thus would require a precision on the ratio of branching fractions of 5% or better to match the current determination based on R_b and γ , and 2.5% or better to match the current determination based on R_b , Δm_d and Δm_s .

A second future application for the ratio of branching fractions between $B_d^0 \rightarrow \mu^+ \mu^-$ and $B_s^0 \rightarrow \mu^+ \mu^-$ is the quantity [77]

$$U_{\mu\mu}^{ds} \equiv \sqrt{\frac{|P_{\mu\mu}^d|^2 + |S_{\mu\mu}^d|^2}{|P_{\mu\mu}^s|^2 + |S_{\mu\mu}^s|^2}}, \quad (128)$$

$$= \left[\frac{\tau_{B_s} (1 - y_d^2) (1 + \mathcal{A}_{\Delta\Gamma}^d y_d) \sqrt{m_{B_s}^2 - 4m_\mu^2}}{\tau_{B_d} (1 - y_s^2) (1 + \mathcal{A}_{\Delta\Gamma}^s y_s) \sqrt{m_{B_d}^2 - 4m_\mu^2}} \left(\frac{f_{B_s}}{f_{B_d}} \right)^2 \left| \frac{V_{ts}}{V_{td}} \right|^2 \frac{\bar{\mathcal{B}}(B_d \rightarrow \mu^+ \mu^-)}{\bar{\mathcal{B}}(B_s \rightarrow \mu^+ \mu^-)} \right]^{1/2}. \quad (129)$$

It has the advantage over the individual $B_d^0 \rightarrow \mu^+ \mu^-$ and $B_s^0 \rightarrow \mu^+ \mu^-$ branching fraction measurements that common parameters and uncertainties drop out in the ratio. Therefore it provides a more powerful test of the SM, where $U_{\mu\mu}^{ds} = 1$.

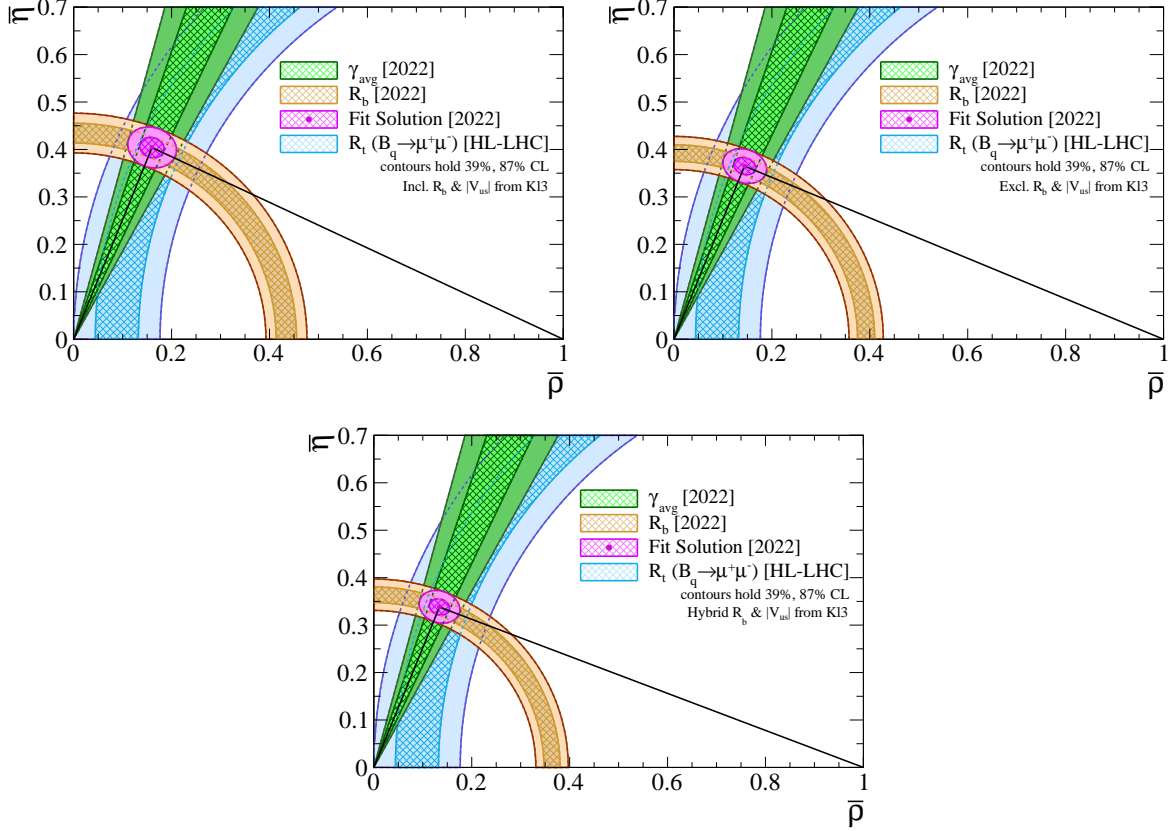


Figure 14: Comparison between the current SM determination of the UT apex and the expected constraint for the LHCb Upgrade II on R_t from the ratio of branching fractions of $B_d^0 \rightarrow \mu^+ \mu^-$ and $B_s^0 \rightarrow \mu^+ \mu^-$. Left: Inclusive scenario. Right: Exclusive scenario. Bottom: Hybrid scenario.

7 Conclusions

In this paper, we have presented a comprehensive study of NP in $B_q^0 - \bar{B}_q^0$ mixing. Our main goal is to determine the allowed parameter space for NP, having a critical look at analyses of the determination of the UT apex, which is needed as input for the corresponding SM predictions. In particular, we explore the impact of the discrepancies between inclusive and exclusive measurements of the CKM matrix elements $|V_{ub}|$ and $|V_{cb}|$, which allow us to fix the side R_b of the UT. Specifically, we perform separate analyses for the inclusive and exclusive determinations, respectively, and for a hybrid scenario, which combines the exclusive $|V_{ub}|$ with the inclusive $|V_{cb}|$ value. Generally, we find sizeable differences between these combinations, demonstrating that it would be very desirable and important to finally resolve the tensions between inclusive and exclusive determinations of the CKM parameters.

Combining the R_b side with information on the angle γ , we can determine the apex of the UT. This angle is usually determined through $B \rightarrow DK$ decays, which proceed only via tree topologies. In our analysis, we utilise another avenue to obtain information on γ , which is provided by $B \rightarrow \pi\pi$, $\rho\pi$, $\rho\rho$ modes and isospin relations allowing us to control penguin uncertainties. Typically, these measurements are interpreted in terms of the UT angle α . However, using information on the mixing phase ϕ_d , they actually

determine γ . Interestingly, we find full agreement between these two determinations of γ , which is non-trivial in view of the different dynamics governing the corresponding decays. Within the SM, such an agreement is expected. Should a discrepancy arise in the future, it would indicate NP contributions to the corresponding decay amplitude, thereby requiring a more involved analysis. In view of the current agreement, we make an average between the two values and assume that this is the SM value of γ .

Using this information on R_b and γ , we perform determinations of the UT apex for the various determinations of the CKM matrix elements $|V_{ub}|$ and $|V_{cb}|$. Furthermore, within the SM, indirect CP violation in the neutral kaon system, described by the observable $|\varepsilon_K|$, allows us to obtain another constraint on the UT apex, given by a hyperbola in the $\bar{\rho}-\bar{\eta}$ plane. This curve depends strongly on $|V_{cb}|$, thereby suggesting a probe to distinguish between the inclusive and exclusive determinations of this CKM element. In our analysis, we find indeed this feature: the exclusive case gives sizeable tension, the inclusive case is more consistent, while the hybrid scenario results in the most compatible picture with the UT apex. Due to this strong dependence, it will be interesting to see how the interplay between the $|\varepsilon_K|$ hyperbola and the UT apex will evolve in the future.

The determination of the UT from R_b and γ plays a key role for the SM predictions of the $B_q^0-\bar{B}_q^0$ mixing parameters. It is important to stress that the corresponding UT analysis does not depend on any information from $B_q^0-\bar{B}_q^0$ mixing. We find that the choice of input parameters – inclusive, exclusive or hybrid – significantly impacts the picture emerging for the NP parameters in $B_q^0-\bar{B}_q^0$ mixing.

First, we constrain in a model-independent way the NP parameters separately for B_s and B_d systems. The strongest evidence for NP would arise in the B_s system for the exclusive CKM matrix elements, corresponding to a NP contribution of about 20% with a significance of 3.5 standard deviations.

Next, we consider a flavour universal scenario with equal NP contributions to the B_d and B_s systems. In such a situation, the NP effects would cancel in the ratio $\Delta m_d/\Delta m_s$. Consequently, we could use it to fix the side R_t of the UT. Combining this side with R_b allows us then to determine the UT apex without any information on γ . We find a picture very similar to the situation in the fit for the B_s system, implying that this system dominates the analysis. While in the exclusive case the fit regions overlap well with those for the general NP analysis for the B_s system, we find that the shapes of the contours for B_d and B_s systems are very different for the inclusive and hybrid scenarios, thereby indicating that the flavour universal scenario might not be realised in nature. However, in view of the current uncertainties, we cannot rule out such kind of NP.

Finally, we go beyond the flavour universal scenario and relax the corresponding assumption when determining the NP parameters. While we still use the ratio $\Delta m_d/\Delta m_s$ to determine the UT apex together with the information on R_b , we extract κ_q, σ_q separately using the individual measurements of Δm_q and ϕ_q . We find that the solutions for the B_d and B_s systems are statistically compatible with each other, but do not look the same. Consequently, the data favour a NP scenario which is not flavour universal in this analysis, although it cannot be excluded with the current precision. Let us finally emphasize that this analysis does not require information on γ . It will be interesting to see how the picture for the NP parameters will evolve in the future.

Our results for the NP parameters in the B_s system can be applied to the analysis of the rare leptonic decay $B_s^0 \rightarrow \mu^+\mu^-$. The corresponding SM branching ratio, using unitarity of the CKM matrix, depends on the CKM element $|V_{cb}|$. We have explored

the impact of different determinations of this quantity, finding that it plays the key role for the uncertainty of the SM branching ratio. This dependence can be eliminated through the ratio of the $B_s^0 \rightarrow \mu^+\mu^-$ branching ratio with the mass difference Δm_s . We generalise this approach by including possible NP contributions to $B_s^0\text{--}\bar{B}_s^0$ mixing through our analysis and constrain the space for NP in $B_s^0 \rightarrow \mu^+\mu^-$ through the current measurement of the branching ratio. Following these lines, the CKM factors and the UT apex enter only through the analysis of NP in $B_s^0\text{--}\bar{B}_s^0$ mixing. Another interesting mode is the $B_d^0 \rightarrow \mu^+\mu^-$ decay which has not yet been observed. In the SM, the ratio of the branching ratios of $B_d^0 \rightarrow \mu^+\mu^-$ and $B_s^0 \rightarrow \mu^+\mu^-$ allows us to determine the R_t side of UT. We have illustrated this interesting option for a future scenario, comparing it with the current picture of the UT.

We have extrapolated our analysis of the NP parameters of $B_q^0\text{--}\bar{B}_q^0$ mixing to the future high-precision era by considering various projections for the CKM matrix elements, the UT apex fit and lattice calculations. For the B_d system we find that the SM determination of the UT apex represents a key limitation for the NP searches. On the other hand, the B_s system has no such limitation and looks particularly interesting for revealing new sources of NP. In the future, studies of $B_q^0\text{--}\bar{B}_q^0$ mixing will remain a central element of the analysis to further constrain NP. It will be exciting to obtain the full picture providing links to other probes such as anomalies in semileptonic rare B decays.

Acknowledgements

This research has been supported by the Netherlands Organisation for Scientific Research (NWO). PvV acknowledges support from the DFG through the Emmy Noether research project 400570283, and through the German-Israeli Project Cooperation (DIP).

References

- [1] P. Ball and R. Fleischer, *Probing new physics through B mixing: Status, benchmarks and prospects*, *Eur. Phys. J. C* **48** (2006) 413, [arXiv:hep-ph/0604249](#).
- [2] UTfit Collaboration, M. Bona *et al.*, *The UTfit collaboration report on the status of the unitarity triangle beyond the Standard Model. I. Model-independent analysis and minimal flavor violation*, *JHEP* **03** (2006) 080, [arXiv:hep-ph/0509219](#).
- [3] UTfit Collaboration, M. Bona *et al.*, *Model-independent constraints on $\Delta F = 2$ operators and the scale of new physics*, *JHEP* **03** (2008) 049, [arXiv:0707.0636](#), Updated results and plots are available at <https://utfit.org>.
- [4] A. Lenz *et al.*, *Anatomy of new physics in $B\text{--}\bar{B}$ mixing*, *Phys. Rev. D* **83** (2011) 036004, [arXiv:1008.1593](#).
- [5] A. Lenz *et al.*, *Constraints on new physics in $B\text{--}\bar{B}$ mixing in the light of recent LHCb data*, *Phys. Rev. D* **86** (2012) 033008, [arXiv:1203.0238](#).
- [6] J. Charles *et al.*, *New physics in B meson mixing: future sensitivity and limitations*, *Phys. Rev. D* **102** (2020) 056023, [arXiv:2006.04824](#).

- [7] N. Awasthi *et al.*, *Implications of precision measurements and unitarity on CKM paradigm*, *Int. J. Mod. Phys. A* **36** (2021) 2150208.
- [8] N. Cabibbo, *Unitary symmetry and leptonic decays*, *Phys. Rev. Lett.* **10** (1963) 531.
- [9] M. Kobayashi and T. Maskawa, *CP violation in the renormalizable theory of weak interaction*, *Prog. Theor. Phys.* **49** (1973) 652.
- [10] G. Ricciardi, *Theory: Semileptonic B decays and $|V_{xb}|$ update*, *PoS BEAUTY2020* (2021) 031, [arXiv:2103.06099](#).
- [11] CKMfitter Group, J. Charles *et al.*, *Current status of the Standard Model CKM fit and constraints on $\Delta F = 2$ new physics*, *Phys. Rev. D* **91** (2015) 073007, [arXiv:1501.05013](#), Updated results and plots are available at <https://ckmfitter.in2p3.fr>.
- [12] UTfit Collaboration, M. Bona *et al.*, *The Unitarity Triangle fit in the Standard Model and hadronic parameters from lattice QCD: A reappraisal after the measurements of Δm_s and $BR(B \rightarrow \tau \nu_\tau)$* , *JHEP* **10** (2006) 081, [arXiv:hep-ph/0606167](#), Updated results and plots are available at <https://utfit.org>.
- [13] LHCb Collaboration, R. Aaij *et al.*, *Simultaneous determination of CKM angle γ and charm mixing parameters*, *JHEP* **12** (2021) 141, [arXiv:2110.02350](#).
- [14] J. Brod, A. Lenz, G. Tetlalmatzi-Xolocotzi, and M. Wiebusch, *New physics effects in tree-level decays and the precision in the determination of the quark mixing angle γ* , *Phys. Rev. D* **92** (2015) 033002, [arXiv:1412.1446](#).
- [15] A. Lenz and G. Tetlalmatzi-Xolocotzi, *Model-independent bounds on new physics effects in non-leptonic tree-level decays of B-mesons*, *JHEP* **07** (2020) 177, [arXiv:1912.07621](#).
- [16] S. Iguro and T. Kitahara, *Implications for new physics from a novel puzzle in $\bar{B}_{(s)}^0 \rightarrow D_{(s)}^{(*)+} \{\pi^-, K^-\}$ decays*, *Phys. Rev. D* **102** (2020) 071701, [arXiv:2008.01086](#).
- [17] F.-M. Cai, W.-J. Deng, X.-Q. Li, and Y.-D. Yang, *Probing new physics in class-I B-meson decays into heavy-light final states*, *JHEP* **10** (2021) 235, [arXiv:2103.04138](#).
- [18] M. Bordone, A. Greljo, and D. Marzocca, *Exploiting dijet resonance searches for flavor physics*, *JHEP* **08** (2021) 036, [arXiv:2103.10332](#).
- [19] R. Fleischer and E. Malami, *Using $B_s^0 \rightarrow D_s^\mp K^\pm$ decays as a portal to new physics*, *Phys. Rev. D* **106** (2022) 056004, [arXiv:2109.04950](#).
- [20] R. Fleischer and E. Malami, *Revealing new physics in $B_s^0 \rightarrow D_s^\mp K^\pm$ decays*, [arXiv:2110.04240](#).
- [21] A. J. Buras, *Relations between $\Delta m_{s,d}$ and $B_{s,d} \rightarrow \mu \bar{\mu}$ in models with minimal flavor violation*, *Phys. Lett. B* **566** (2003) 115, [arXiv:hep-ph/0303060](#).
- [22] C. Bobeth and A. J. Buras, *Searching for new physics with $\bar{\mathcal{B}}(B_{s,d} \rightarrow \mu \bar{\mu})/\Delta M_{s,d}$* , *Acta Phys. Polon. B* **52** (2021) 1189, [arXiv:2104.09521](#).

- [23] A. J. Buras and E. Venturini, *Searching for new physics in rare K and B decays without $|V_{cb}|$ and $|V_{ub}|$ uncertainties*, *Acta Phys. Polon. B* **53** (2021) A1, [arXiv:2109.11032](#).
- [24] L. Wolfenstein, *Parametrization of the Kobayashi–Maskawa matrix*, *Phys. Rev. Lett.* **51** (1983) 1945.
- [25] A. J. Buras, M. E. Lautenbacher, and G. Ostermaier, *Waiting for the top quark mass, $K^+ \rightarrow \pi^+ \nu \bar{\nu}$, $B_s^0 - \bar{B}_s^0$ mixing and CP asymmetries in B decays*, *Phys. Rev. D* **50** (1994) 3433, [arXiv:hep-ph/9403384](#).
- [26] Particle Data Group, R. L. Workman *et al.*, *Review of Particle Physics*, *PTEP* **2022** (2022) 083C01, Updated results are available at <http://pdglive.lbl.gov>.
- [27] HFLAV Collaboration, Y. Amhis *et al.*, *Averages of b -hadron, c -hadron, and τ -lepton properties as of 2021*, [arXiv:2206.07501](#), See also <https://hflav.web.cern.ch/>.
- [28] G. Hiller, *Lepton nonuniversality anomalies & implications*, in *53rd Rencontres de Moriond on QCD and High Energy Interactions*, 43–48, 2018, [arXiv:1804.02011](#).
- [29] S. Fajfer, *Theory status - Puzzles in B meson decays and LFU?*, *SciPost Phys. Proc.* **1** (2019) 010.
- [30] F. U. Bernlochner, M. F. Sevilla, D. J. Robinson, and G. Wormser, *Semitauponic b -hadron decays: A lepton flavor universality laboratory*, *Rev. Mod. Phys.* **94** (2022) 015003, [arXiv:2101.08326](#).
- [31] J. Albrecht, D. van Dyk, and C. Langenbruch, *Flavour anomalies in heavy quark decays*, *Prog. Part. Nucl. Phys.* **120** (2021) 103885, [arXiv:2107.04822](#).
- [32] M. Jung and D. M. Straub, *Constraining new physics in $b \rightarrow c \ell \nu$ transitions*, *JHEP* **01** (2019) 009, [arXiv:1801.01112](#).
- [33] G. Banelli, R. Fleischer, R. Jaarsma, and G. Tetlalmatzi-Xolocotzi, *Decoding (pseudo)-scalar operators in leptonic and semileptonic B decays*, *Eur. Phys. J. C* **78** (2018) 911, [arXiv:1809.09051](#).
- [34] S. Iguro and R. Watanabe, *Bayesian fit analysis to full distribution data of $\bar{B} \rightarrow D^{(*)} \ell \bar{\nu}$: $|V_{cb}|$ determination and new physics constraints*, *JHEP* **08** (2020) 006, [arXiv:2004.10208](#).
- [35] R. Fleischer, R. Jaarsma, and G. Tetlalmatzi-Xolocotzi, *Mapping out the space for new physics with leptonic and semileptonic $B_{(c)}$ decays*, *Eur. Phys. J. C* **81** (2021) 658, [arXiv:2104.04023](#).
- [36] M. Z. Barel, K. De Bruyn, R. Fleischer, and E. Malami, *In pursuit of new physics with $B_d^0 \rightarrow J/\psi K^0$ and $B_s^0 \rightarrow J/\psi \phi$ decays at the high-precision frontier*, *J. Phys. G* **48** (2021) 065002, [arXiv:2010.14423](#).
- [37] M. Z. Barel, K. De Bruyn, R. Fleischer, and E. Malami, *Penguin effects in $B_d^0 \rightarrow J/\psi K_S^0$ and $B_s^0 \rightarrow J/\psi \phi$* , in *11th International Workshop on the CKM Unitarity Triangle*, 2022, [arXiv:2203.14652](#).

- [38] LHCb Collaboration, R. Aaij *et al.*, *Measurement of CP asymmetry in $B_s^0 \rightarrow D_s^\mp K^\pm$ decays*, *JHEP* **03** (2018) 059, [arXiv:1712.07428](#).
- [39] M. Gronau and D. London, *Isospin analysis of CP asymmetries in B decays*, *Phys. Rev. Lett.* **65** (1990) 3381.
- [40] J. Charles, O. Deschamps, S. Descotes-Genon, and V. Niess, *Isospin analysis of charmless B-meson decays*, *Eur. Phys. J. C* **77** (2017) 574, [arXiv:1705.02981](#).
- [41] C.-Y. Seng, D. Galviz, W. J. Marciano, and U.-G. Meißner, *Update on $|V_{us}|$ and $|V_{us}/V_{ud}|$ from semileptonic kaon and pion decays*, *Phys. Rev. D* **105** (2022) 013005, [arXiv:2107.14708](#).
- [42] C.-Y. Seng, D. Galviz, M. Gorchtein, and U.-G. Meißner, *Complete theory of radiative corrections to $K_{\ell 3}$ decays and the V_{us} update*, *JHEP* **07** (2022) 071, [arXiv:2203.05217](#).
- [43] Flavour Lattice Averaging Group, Y. Aoki *et al.*, *FLAG review 2021*, [arXiv:2111.09849](#), See also <http://flag.unibe.ch/>.
- [44] M. Bordone, B. Capdevila, and P. Gambino, *Three loop calculations and inclusive V_{cb}* , *Phys. Lett. B* **822** (2021) 136679, [arXiv:2107.00604](#).
- [45] P. Gambino, P. Giordano, G. Ossola, and N. Uraltsev, *Inclusive semileptonic B decays and the determination of $|V_{ub}|$* , *JHEP* **10** (2007) 058, [arXiv:0707.2493](#).
- [46] LHCb Collaboration, R. Aaij *et al.*, *Determination of the quark coupling strength $|V_{ub}|$ using baryonic decays*, *Nature Phys.* **11** (2015) 743, [arXiv:1504.01568](#).
- [47] LHCb Collaboration, R. Aaij *et al.*, *First observation of the decay $B_s^0 \rightarrow K^- \mu^+ \nu_\mu$ and measurement of $|V_{ub}|/|V_{cb}|$* , *Phys. Rev. Lett.* **126** (2021) 081804, [arXiv:2012.05143](#).
- [48] M. Bordone, N. Gubernari, D. van Dyk, and M. Jung, *Heavy-Quark expansion for $\bar{B}_s \rightarrow D_s^{(*)}$ form factors and unitarity bounds beyond the $SU(3)_F$ limit*, *Eur. Phys. J. C* **80** (2020) 347, [arXiv:1912.09335](#).
- [49] A. J. Buras and E. Venturini, *The exclusive vision of rare K and B decays and of the quark mixing in the Standard Model*, *Eur. Phys. J. C* **82** (2022) 615, [arXiv:2203.11960](#).
- [50] LHCb Collaboration, R. Aaij *et al.*, *Measurement of the CKM angle γ from a combination of LHCb results*, *JHEP* **12** (2016) 087, [arXiv:1611.03076](#), The Gamma-Combo package is available from <https://gammacombo.github.io>.
- [51] J. Brod, M. Gorbahn, and E. Stamou, *Standard-Model prediction of ϵ_K with manifest quark-mixing unitarity*, *Phys. Rev. Lett.* **125** (2020) 171803, [arXiv:1911.06822](#).
- [52] A. J. Buras, D. Guadagnoli, and G. Isidori, *On ϵ_K beyond lowest order in the operator product expansion*, *Phys. Lett. B* **688** (2010) 309, [arXiv:1002.3612](#).

- [53] T. Inami and C. S. Lim, *Effects of superheavy quarks and leptons in low-energy weak processes $K_L \rightarrow \mu\bar{\mu}$, $K^+ \rightarrow \pi^+\nu\bar{\nu}$ and $K^0 \leftrightarrow \bar{K}^0$* , *Prog. Theor. Phys.* **65** (1981) 297, [Erratum: *Prog.Theor.Phys.* 65, 1772 (1981)].
- [54] K. G. Chetyrkin, J. H. Kuhn, and M. Steinhauser, *RunDec: A Mathematica package for running and decoupling of the strong coupling and quark masses*, *Comput. Phys. Commun.* **133** (2000) 43, [arXiv:hep-ph/0004189](#).
- [55] B. Schmidt and M. Steinhauser, *CRunDec: A C++ package for running and decoupling of the strong coupling and quark masses*, *Comput. Phys. Commun.* **183** (2012) 1845, [arXiv:1201.6149](#).
- [56] J. Brod, S. Kvedaraite, and Z. Polonsky, *Two-loop electroweak corrections to the top-quark contribution to ε_K* , *JHEP* **12** (2021) 198, [arXiv:2108.00017](#).
- [57] CDF Collaboration, T. Aaltonen *et al.*, *High-precision measurement of the W boson mass with the CDF II detector*, *Science* **376** (2022) 170.
- [58] J. Brod, S. Kvedaraite, Z. Polonsky, and A. Youssef, *Electroweak corrections to the charm-top-quark Contribution to ϵ_K* , [arXiv:2207.07669](#).
- [59] A. J. Buras, M. Jamin, and P. H. Weisz, *Leading and next-to-leading QCD corrections to ϵ -parameter and $B^0-\bar{B}^0$ mixing in the presence of a heavy top quark*, *Nucl. Phys. B* **347** (1990) 491.
- [60] G. Buchalla, A. J. Buras, and M. E. Lautenbacher, *Weak decays beyond leading logarithms*, *Rev. Mod. Phys.* **68** (1996) 1125, [arXiv:hep-ph/9512380](#).
- [61] R. J. Dowdall *et al.*, *Neutral B -meson mixing from full lattice QCD at the physical point*, *Phys. Rev. D* **100** (2019) 094508, [arXiv:1907.01025](#).
- [62] P. Gambino, A. Kwiatkowski, and N. Pott, *Electroweak effects in the $B^0-\bar{B}^0$ mixing*, *Nucl. Phys. B* **544** (1999) 532, [arXiv:hep-ph/9810400](#).
- [63] LHCb Collaboration, R. Aaij *et al.*, *Precise determination of the $B_s^0-\bar{B}_s^0$ oscillation frequency*, *Nature Phys.* **18** (2022) 1, [arXiv:2104.04421](#).
- [64] L. Di Luzio, M. Kirk, A. Lenz, and T. Rauh, *ΔM_s theory precision confronts flavour anomalies*, *JHEP* **12** (2019) 009, [arXiv:1909.11087](#).
- [65] LHCb Collaboration, R. Aaij *et al.*, *Analysis of neutral B -meson decays into two muons*, *Phys. Rev. Lett.* **128** (2022) 041801, [arXiv:2108.09284](#).
- [66] A. J. Buras, J. Girrbach, D. Guadagnoli, and G. Isidori, *On the Standard Model prediction for $\mathcal{B}(B_{s,d} \rightarrow \mu^+\mu^-)$* , *Eur. Phys. J. C* **72** (2012) 2172, [arXiv:1208.0934](#).
- [67] A. J. Buras, R. Fleischer, J. Girrbach, and R. Knegjens, *Probing new physics with the $B_s \rightarrow \mu + \mu -$ time-dependent rate*, *JHEP* **07** (2013) 077, [arXiv:1303.3820](#).
- [68] K. De Bruyn *et al.*, *Probing new physics via the $B_s^0 \rightarrow \mu^+\mu^-$ effective lifetime*, *Phys. Rev. Lett.* **109** (2012) 041801, [arXiv:1204.1737](#).

- [69] M. Beneke, C. Bobeth, and R. Szafron, *Power-enhanced leading-logarithmic QED corrections to $B_q \rightarrow \mu^+ \mu^-$* , [JHEP **10** \(2019\) 232](#), [arXiv:1908.07011](#).
- [70] ATLAS Collaboration, M. Aaboud *et al.*, *Study of the rare decays of B_s^0 and B^0 mesons into muon pairs using data collected during 2015 and 2016 with the ATLAS detector*, [JHEP **04** \(2019\) 098](#), [arXiv:1812.03017](#).
- [71] CMS Collaboration, A. M. Sirunyan *et al.*, *Measurement of properties of $B_s^0 \rightarrow \mu^+ \mu^-$ decays and search for $B^0 \rightarrow \mu^+ \mu^-$ with the CMS experiment*, [JHEP **04** \(2020\) 188](#), [arXiv:1910.12127](#).
- [72] CMS Collaboration, *Measurement of $B_s^0 \rightarrow \mu^+ \mu^-$ decay properties and search for the $B^0 \rightarrow \mu \mu$ decay in proton-proton collisions at $\sqrt{s} = 13$ TeV*, [CMS PAS BPH-21-006](#).
- [73] L.-S. Geng *et al.*, *Implications of new evidence for lepton-universality violation in $b \rightarrow s \ell^+ \ell^-$ decays*, [Phys. Rev. D **104** \(2021\) 035029](#), [arXiv:2103.12738](#).
- [74] W. Altmannshofer and P. Stangl, *New physics in rare B decays after Moriond 2021*, [Eur. Phys. J. C **81** \(2021\) 952](#), [arXiv:2103.13370](#).
- [75] T. Hurth, F. Mahmoudi, D. M. Santos, and S. Neshatpour, *More indications for lepton nonuniversality in $b \rightarrow s \ell^+ \ell^-$* , [Phys. Lett. B **824** \(2022\) 136838](#), [arXiv:2104.10058](#).
- [76] LHCb Collaboration, R. Aaij *et al.*, *Physics case for an LHCb Upgrade II - Opportunities in flavour physics, and beyond, in the HL-LHC era*, [arXiv:1808.08865](#).
- [77] R. Fleischer, R. Jaarsma, and G. Tetlalmatzi-Xolocotzi, *In pursuit of new physics with $B_{s,d}^0 \rightarrow \ell^+ \ell^-$* , [JHEP **05** \(2017\) 156](#), [arXiv:1703.10160](#).